DESIGN OF WIDEBAND LINEAR PHASE SURFACE ACOUSTIC WAVE FILTERS

DESIGN OF WIDEBAND LINEAR PHASE SURFACE ACOUSTIC WAVE FILTERS

by

NICHOLAS JOHN SLATER, B.Eng.

A Thesis

Submitted to the Faculty of Graduate Studies

In Partial Fullfillment of the Requirements

for the Degree

Master of Engineering

McMaster University

June, 1982

MASTER OF ENGINEERING (1982) McMaster University

(Electrical Engineering) Hamilton, Ontario

Title: Design of Wideband Linear Phase Surface Acoustic Wave Filters

Author: Nicholas John Slater, B.Eng. (McMaster University)

Supervisor: Professor C.K. Campbell

Number of Pages: ix, 108

Scope and Contents: The proposed design of wideband linear phase SAW filters using curved finger transducers and distortion minimizing techniques.

ABSTRACT

A two-part scheme for the design of wideband linear phase SAW filters is proposed. The design uses curved finger interdigital transducers, and extension of slanted finger design, to compensate for circuit effects and eliminate the need for matching. Theory is combined with distortion minimizing techniques to realize devices which satisfy INTELSAT filter specifications.

Basic SAW theory is reviewed and curved finger theory presented, while methods of distortion minimization are both reviewed and proposed. Experimental results which illustrate and support the theory given are included.

ACKNOWLEDGEMENTS

The author wishes to express his appreciation to Dr. C.K. Campbell for his constant guidance throughout this rewarding experience. As a supervisor, he strikes a harmonious balance between administration and collaboration; his own drive and motivation are contagious and the test facilities provided are top of the line.

Thanks are extended to Mr. Alfred Zeuner for his close association and partnership, Mr. Joseph Sferrazza-papa for his practical advice, Mr. Yanglin Ye for his insight and encouragement and to Mr. Mark Usik and Mr. Peter Edmonsen for their able technical assistance.

The author also acknowledges the capable staff of the Engineering Word Processing Centre for typing of this manuscript.

Finally the author wishes to thank his parents for their tacit yet deeply-felt support in this and other endeavours.

TABLE OF CONTENTS

LIST OF FIGURES

LIST OF FIGURES (cont'd)

CHAPTER 1

BASIC SAW THEORY

1.1 Introduction

The surface acoustic wave (SAW) bandpass filter is a form of transversal filter developed by Kalman in the 1940's.[21] The use of transversal filters at high frequency had been severely handicapped until the advent of SAW devices due to the need for adequate delay elements. Kalman used lengths of coaxial cable which, to say the least, were impractical; lengths of a few metres are necessary to provide a wavelength delay at 70 MHz. The speed of acoustic waves in most useful materials is 10^5 times smaller than the speed of electromagnetic waves giving a proportionate reduction in wavelength for a given frequency. Kalman's interest in transversal filters was spurred by the need for filters with linear phase (constant group delay), which is inherent for any symmetrical transversal filter as is shown in section 1.3.

1.2 Scope of this Thesis

The need for good phase linearity over a wide bandwidth is ever more present today, when bandwidth constraints are tight. Many schemes for minimization of necessary bandwidth to convey a given amount of information are in use and it is of critical importance that bandwidth is not wasted due to filter distortion.

Specifications published by INTELSAT for filters to be used in

earth stations have strict limitations on the deviations from linear phase, passband ripple and sideband suppression. These specifications are shown in Figure 1.1 and Table 1.1 a) and b).

With conventional SAW filters, however, a trade-off exists between bandwidth and insertion loss. Furthermore, for very wide bandwidth filters, matching becomes increasingly difficult. These restrictions have been tackled by Campbell et al.[3], by the introduction of a novel slanted finger design which superposes the effect of many narrowband filters with adjacent centre frequencies to create a single wideband filter. Although the wideband is achieved with only moderate insertion loss, problems still exist, predominantly the appearance of a sloping passband response as opposed to the desired flat response. Campbell solved this problem by providing external compensation in the form of a shunt inductor, but such a component increases the complexity, cost and size of the design.

Sources of distortion in SAW devices are fairly well known and possible solutions have been proposed which will be presented in the following sections.

The purpose of this thesis, then, is:

1) to determine the cause of and propose solutions to the sloping passband response in SAW filters of up to 50% fractional bandwidth.

2) to investigate the distortion mechanisms in SAW filters and determine whether distortion can be reduced sufficiently to satisfy the constraints of the specifications in Figure 1.1.

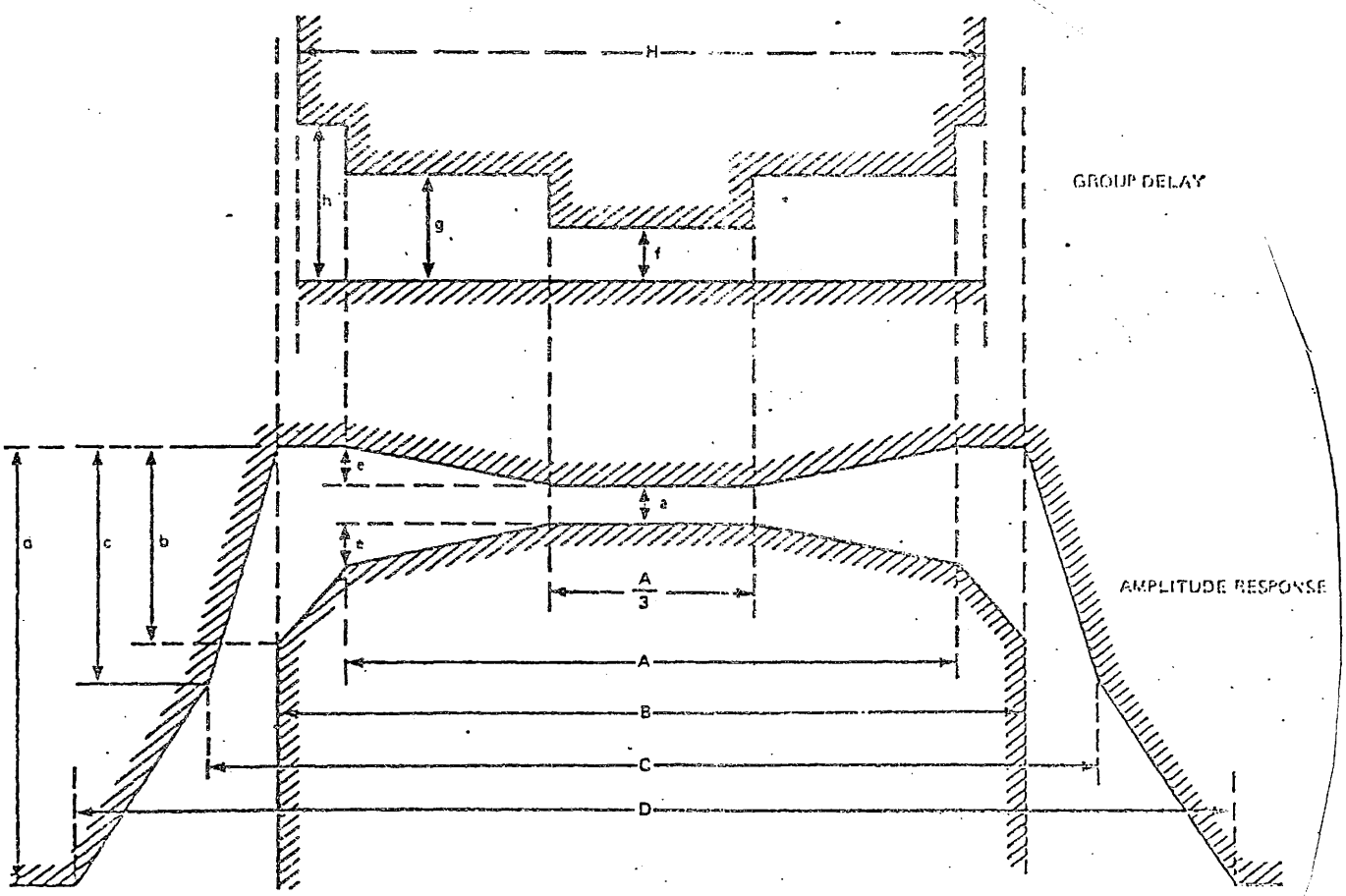

NOTES: (1) FIGURES ARE SYMMETRICAL RELATIVE TO CENTER FREQUENCY
(2) FIGURES ARE NOT DRAWN TO SCALE
(3) AMPLITUDE SCALE IS LINEAR IN dB
(4) FREQUENCY SCALE IS LINEAR IN MHz

G-15633

f_c=70MHz

Figure 1.1

Transmit Amplitude and Group Delay Requirements, Earth Station Total

Table 1.1 a)
Transmit Equipment
Group Delay Characteristics

CARRIER SIZE (MHz)	A (MHz)	H (MHz)	f (ns)	g (ns)	h (ns)
1.25	0.9	1.3	1/24	1/24	1/30
2.5	1.8	3.1	16	16	20
5.0	3.6	4.1	12	12	20
7.5	5.4	6.9	12	12	20
10.0	7.2	8.3	8	8	16
15.0	10.8	12.4	6	6	15
17.5	12.6	14.2	6	6	15
20.0	14.4	16.6	4	5	15
25.0	18.0	20.7	3	5	15
→ 36.0	28.8	33.1	3	5	15
Video*	12.6	14.2	6	6	15
Video**	24.0	30.0	5	5	15

f_c=70MHz

Table 1.1 b)
Transmit Equipment
Gain/Frequency Characteristics

CARRIER SIZE (MHz)	A (MHz)	B (MHz)	C (MHz)	D (MHz)	a (dB)	b (dB)	c (dB)	d (dB)	e (dB)
1.25	0.9	1.1	1.50	4.0	0.1	1.5	3.0	25	0.0
2.5	1.8	2.25	2.75	8.0	0.1	1.5	2.5	25	0.0
5.0	3.6	4.50	5.25	13.0	0.5	2.0	3.0	25	0.0
7.5	5.4	6.75	7.75	17.0	0.4	2.5	4.0	25	0.0
10.0	7.2	9.00	10.25	19.0	0.3	2.5	5.0	25	0.1
→ 15.0	10.8	13.50	15.50	25.0	0.3	2.5	5.5	25	0.1
17.5	12.6	15.75	18.00	26.5	0.3	2.5	6.5	25	0.1
20.0	14.4	18.00	20.50	28.0	0.3	2.5	7.5	25	0.1
25.0	18.0	22.50	25.75	34.0	0.3	2.5	8.0	25	0.2
→ 36.0	28.8	36.00	45.25	60.0	0.6	2.5	10.0	25	0.3
Video*	12.6	15.75	18.00	26.5	0.3	2.5	6.5	25	0.1
→ Video**	24.0	30.0	***	***	0.5	2.5	***	***	0.3

*Video with characteristics per Table 3.17(b).
**Video with characteristics per Table 3.17(a).
***There is no out-of-band filtering requirements at the transmit earth station. The recommended receiver noise bandwidth is given in Table 3.17(a).

3) to publish results which lend credence to the proposed solutions.

4) to outline the course of future work to further verify, and expand on, the recommendations made.

Towards this end, the rest of this Chapter reviews the current applicable theory of SAW filters. New theory is introduced in the second chapter. Distortion mechanisms are covered in Chapter 3. Chapter 4 describes the fabrication techniques used in constructing the experimental filters, and Chapter 5 presents the results of these experiments and the conclusions and recommendations based on the studies conducted.

1.3 Transversal Filters

Before embarking on a study of basic SAW theory, a brief review of transversal filters is in order both for the insight they provide into SAW work and for two important theorems which are directly applicable to SAW filters.

Contrary to conventional LC filter theory, transversal filters are most easily understood from time domain considerations. As shown in Figure 1.2, the output of a transversal filter y(t) is a superposition of the weighted outputs of a series of delay elements fed by input x(t). This can be expressed mathematically for N delay elements as

$$y(t) = \sum_{n=1}^{N} a_n \, x(t-T_n) \qquad (1.3.1)$$

where a_n is the n^{th} weighting coefficient

and T_n is the (cumulative) n^{th} delay time.

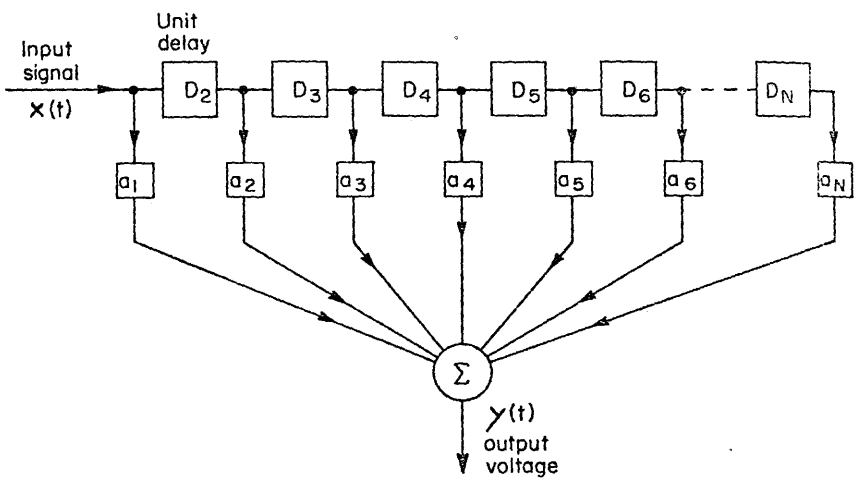

Figure 1.2 Schematic diagram of a transversal filter showing the signal flow from input to output. The delay D_1 is taken as zero delay and is not shown. Copyright 1974 by The Institute of Electrical and Electronic Engineers, Inc. Reprinted, with permission, from *IEEE Trans.* **SU-21,** 1974, p. 13.

For finite N this filter is called a finite impulse response (FIR) filter due to the truncation in the number of "samples" in the time domain upon which the output y(t) is based.

The corresponding frequency domain operation to a shift in the time domain is multiplication by a phase factor $\exp(-j\omega T_n)$ as can be seen from

$$Y(\omega) = \sum_{n=1}^{N} a_n \int_{-\infty}^{\infty} x(t-T_n) \exp(-j\omega t)\, dt$$

$$= \sum_{n=1}^{N} a_n \exp(-j\omega T_n)\, X(\omega)$$

$$= H(\omega)\, X(\omega) \qquad (1.3.2)$$

where $Y(\omega)$ is the Fourier transform of $y(t)$

$X(\omega)$ is the Fourier transform of $x(t)$

The frequency response of the filter can be identified from (1.3.2) as $H(\omega)$ where

$$H(\omega) = \sum_{n=1}^{N} a_n \exp(-j\omega T_n) \qquad (1.3.3)$$

Two theorems follow immediately from this analysis provided the coefficients a_n are real. For convenience, assuming N odd, the frequency response will be written as

$$H(\omega) = \sum_{n=-NP}^{NP} a_n \exp(-j\omega T_n) \qquad (1.3.4)$$

where NP is the number of finger pairs: NP = (N-1)/2

Theorem 1.

For a symmetric filter $a_n = a_{-n}$, $T_n = 2T_o - T_{-n}$

the frequency response is linear phase.

Proof:

$$H(\omega) = \sum_{n=1}^{NP} a_n \exp(-j\omega T_n) + a_o \exp(-j\omega T_o) + \sum_{n=-NP}^{-1} a_n \exp(-j\omega T_n)$$

$$= \exp(-j\omega T_o) \{a_o + \sum_{n=1}^{NP} a_n \exp[-j\omega(T_n - T_o)]$$

$$+ \sum_{n=1}^{NP} a_n \exp[-j\omega(T_o - T_n)]\}$$

$$= \exp(-j\omega T_o) \{a_o + \sum_{n=1}^{NP} 2a_n \cos[\omega(T_n - T_o)]\} \qquad (1.3.5)$$

Since the summed quantity is real, the phase of the filter is simply the phase of the factor $\exp(-j\omega T_o)$ which is linear in frequency.

Theorem 2.

For a filter with constant delay between samples $T_n = \pi n/\omega_o$, the magnitude of the frequency response is symmetrical about the centre frequency, ω_o.

Proof:

$$H(\omega+\Delta\omega) = \sum_{n=-NP}^{NP} a_n \exp[-j(\omega_o+\Delta\omega)\ \pi n/\omega_o]$$

$$= \sum_{n=-NP}^{NP} a_n \exp[-j\Delta\omega\ \pi n/\omega_o] \exp(-j\pi n) \qquad (1.3.6)$$

$$H(\omega-\Delta\omega) = \sum_{n=-NP}^{NP} a_n \exp[-j(\omega_o-\Delta\omega)\ \pi n/\omega_o]$$

$$= \sum_{n=-NP}^{NP} a_n \exp[j\Delta\omega\ \pi n/\omega_o] \exp(-j\pi n) \qquad (1.3.7)$$

Then $H(\omega_o-\omega) = H^*(\omega_o+\omega)$, since $\exp(-j\pi n) = \exp(j\pi n) = (-1)^n$

or $|H(\omega_o-\omega)| = |H(\omega_o+\omega)|$ and the filter is symmetric about ω_o.

These theorems are adaptations of those found in Tancrell.[21]

1.4 The Interdigital Transducer

The transversal filter basis in SAW devices is the interdigital transducer (IDT). Thin parallel conducting strips are deposited on a piezoelectric substrate as shown in Figure 1.3. Alternate strips or "fingers" are connected to opposite-polarity bus bars so that the input voltage appears across each pair of electrodes. The voltage induces a strain in the piezoelectric material; if an alternating voltage is applied a mechanical wave is set up in the material which travels away from the transducer in both directions perpendicular to the fingers. A similar transducer can be used further along the material which detects the mechanical wave by the inverse piezoelectric effect.

The analogy to transversal filters was originated by Tancrell.[21] He noted that the edges of each electrode were regions of highest electric field gradient, which is the driving force for piezoelectric interaction. Thus, the overall effect of each electrode is predominantly due to a highly localized region near the electrode edge, and can be replaced by a simple delta function. This delta function

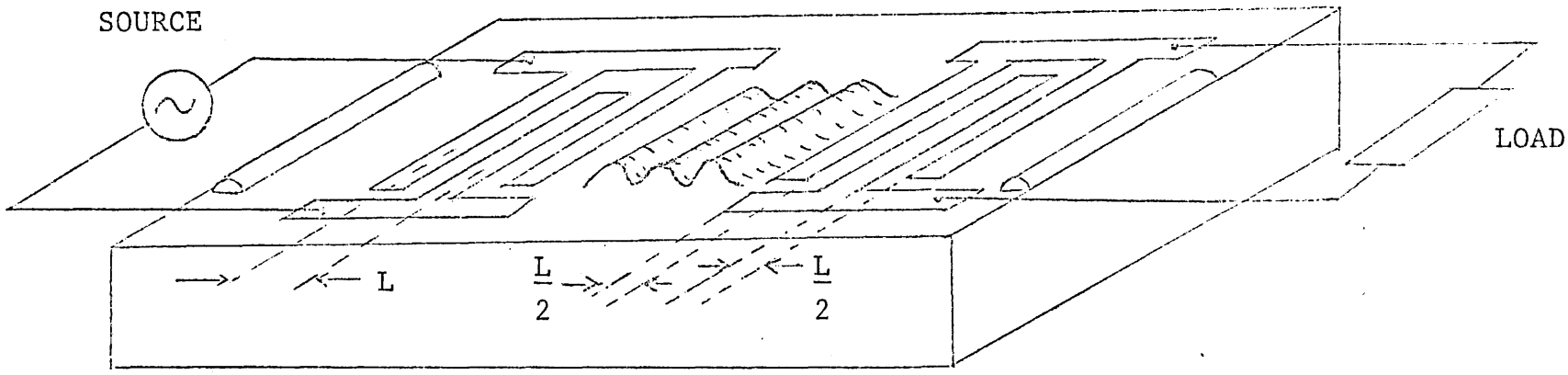

Figure 1.3 Transmitting and Receiving Interdigital Transducers on the surface of a piezoelectric substrate. **(13)**

would have amplitude corresponding to the acoustic power generated or detected by the electrode. The frequency response of the entire transducer, then, would be the sum of the responses of each electrode multiplied by an appropriate phase factor to account for the acoustic time delay between electrodes as in equation (1.3.3). This approach is commonly referred to as the Delta Function Model for SAW filter analysis.

The strength of the acoustic wave depends on the coupling constant of the material, k^2, the capacitance per metre of the electrode pairs, C_s, and, of course, the strength of the input signal. The separation between the fingers constitutes the delay in the analogous transversal filter while the weighting coefficients are determined by the acoustic aperture or extent of finger overlap. Conventional SAW filters generally use apodized transducers in which the overlap changes from finger pair to finger pair. This apodization is comparable to the use of windows in digital filters. Windows provide a means of increasing sideband suppression while decreasing transition bandwidth.

If the finger spacing is constant, a synchronous frequency, f_o, can be identified which, by the second theorem of section 1.3, is the centre frequency of the transducer response.

$$f_o = v_a/(2L) \qquad (1.4.1)$$

where L is the finger separation and v_a the acoustic velocity. The proportion of metallized region to finger separation is called the metallization ratio, η. This ratio influences the finger pair capacitance and determines the suppression of harmonics of the synchronous

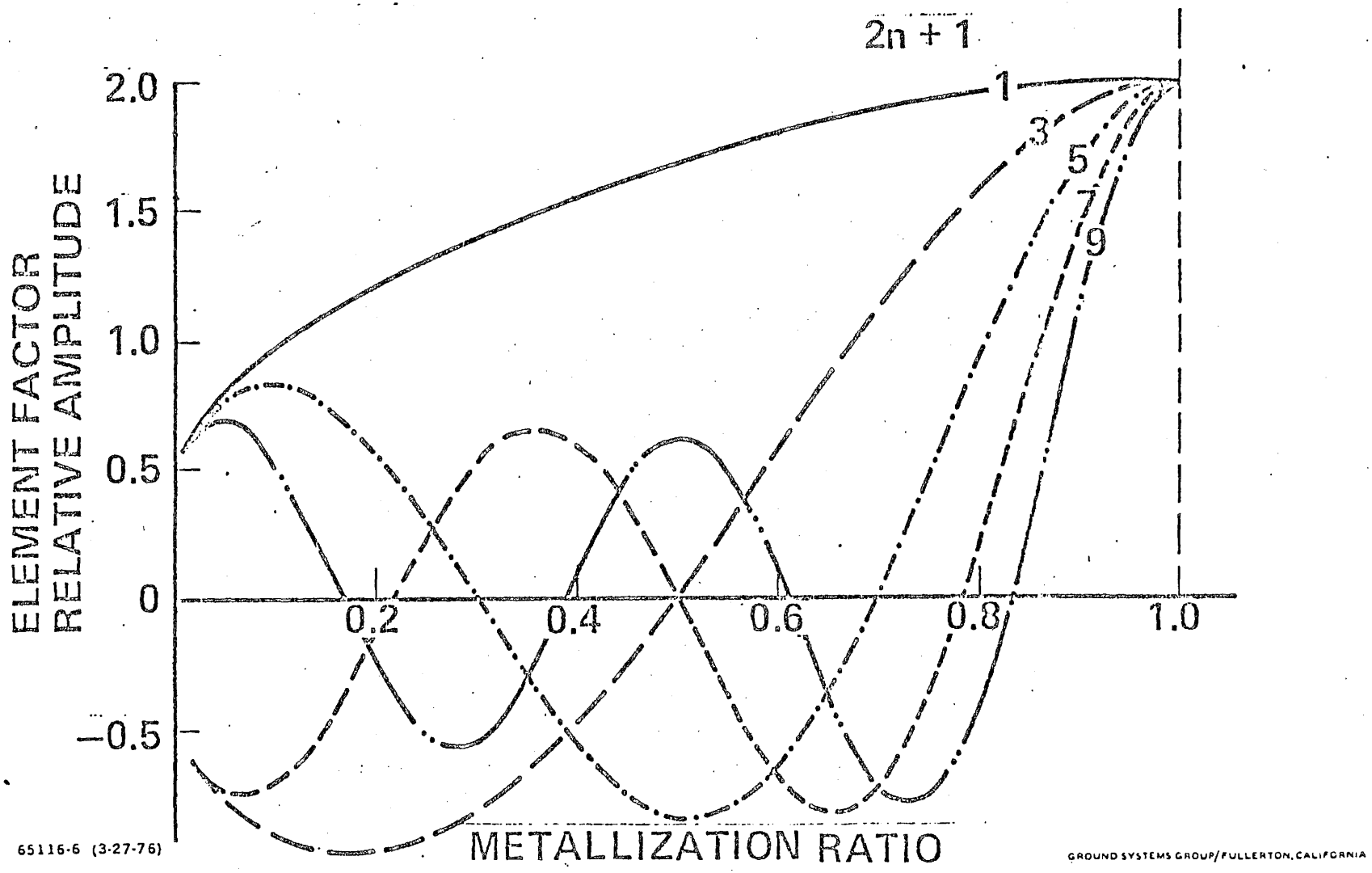

Figure 1.4 Amplitude of the five lowest spatial harmonics as a function of η for the 2-finger geometry transducer. (13)

frequency. Due to the alternating potential of the two-finger period geometry, no even harmonics are launched by the interdigital transducer. Odd harmonics propagate with amplitudes shown in Figure 1.4. It can be shown[13] that the relative amplitude of the $(2n+1)^{th}$ harmonic is proportional to

$$A_{2n+1} = P_n [\cos \pi(1-\eta)] \tag{1.4.2}$$

where P_n is the n^{th} Legendre function of the first kind.

For $\eta = 1/2$, equation (1.4.2) becomes

$$\begin{aligned} A_{2n+1} = P_n(0) &= (-1)^{n/2}\, n!/(n!!)^2 \quad && n \text{ even} \\ &= 0 && n \text{ odd} \end{aligned} \tag{1.4.3}$$

This case of equal metal/gap width is of particular interest since the 3rd, 7th, 11th, etc., harmonics are completely absent. The first harmonic present, then, is the 5th with only half the amplitude of the fundamental due to this factor. (Other factors are present which cause the amplitude of the 5th harmonic to be approximately .523 times that of the fundamental; the Legendre polynomials serve only to show the harmonics which are reduced to zero; they are not intended to represent the relative amplitudes.)

1.5 Surface Acoustic Wave Filters

The delta function model discussed in section 1.4 serves the important purpose of providing the link between transversal filters and SAW filters. Thus, work done in the transversal filter field is more or less directly applicable to SAW filters. The delta function model has its limitations, however, in that the form of the weighting coefficients

in terms of crystal and geometrical parameters is dependent on more advanced models.

The exact field analysis of surface acoustic waves in piezoelectric media subject to mechanical and electromagnetic boundary conditions is well covered by Farnell.[5] The resulting solutions verify the existence of surface waves and allow calculation of parameters, such as wave propagation velocity and penetration depth in terms of crystal properties and driving frequency. However, the overhead of computer time and the inflexibility in view of the nature of numerical solutions make this approach impractical for filter synthesis.

A common approximation made is to assume the electric field in the actual material is either parallel (in-line) or perpendicular (cross-field) to the direction of acoustic wave propagation. In this way, the equivalent circuit representation of crystals excited across either their length or their thickness respectively, as found by Mason[9], are applicable. The details of this approach can be found in Smith.[18]

The technique employed in this thesis represents a compromise between the simplicity of the delta function model and the scope of the advanced circuit model. Formulated by Hartmann[6], the impulse model uses the circuit model and dimensional analysis to determine the dependence of the impulse response of an elementary interdigital transducer on substrate and geometrical parameters. The response of a more complex IDT can be developed by decomposition into and superposition of these elementary strips.

Using the impulse model, the frequency response of the elementary

transducer and the elementary SAW filter are determined in the following sections.

1.5.1 Impulse Response of the Elementary Interdigital Transducer

As implied in the last section, once the mechanical and electromagnetic boundary conditions are defined for an elementary IDT, the potential and acoustic wave amplitude can be written as a sum of eigenfunctions which usually take the form of exponentially damped Fourier components. The fundamental period of these Fourier components is given by the interdigital period or its inverse, the synchronous frequency, discussed in Section 1.4. This fundamental component alone should provide a sufficient analytical base since this thesis is concerned with linear filters of less than 66% bandwidth, effectively out of range of any harmonic interaction. Hartmann[6] shows that the fundamental impulse response of an elementary N+1 finger transducer of aperture Δx is given by

$$\begin{aligned} h(t) &= (16k^2 C_s \Delta x f_o^3)^{1/2} \sin(2\pi f_o t) \qquad -N\tau/2 \leq t \leq N\tau/2 \\ &= 0 \qquad\qquad\qquad\qquad\qquad\qquad\qquad\qquad \text{else} \end{aligned} \tag{1.5.1}$$

where $\tau = 1/(2f_o)$

Here, the time origin has been located, for convenience, at the centre electrode of the configuration.

1.5.2 Frequency Response of the Elementary Interdigital Transducer

The impulse response of an elementary N+1 finger interdigital transducer (IDT) was considered in the last section. From this impulse

response, the frequency response is easily found using the Fourier transform:

$$H(f) = \int_{-\infty}^{\infty} h(t)\exp(-2\pi jft)dt \qquad (1.5.2)$$

Substitution of equation (1.5.1) yields

$$H(f) = (k^2C_s\Delta xf_o)^{1/2}\ 4f_o \int_{-N/(4f_o)}^{N/(4f_o)} \sin(2\pi f_o t)\ \exp(-2\pi jft)dt$$

$$= (k^2C_s\Delta xf_o)^{1/2}\ (-j2f_o) \int_{-N/(4f_o)}^{N/(4f_o)} \{\exp[-2\pi jt(f - f_o)]$$

$$- \exp[-2\pi jt(f + f_o)]\}dt$$

$$= (k^2C_s\Delta xf_o)^{1/2}\ (-j2f_o)\ \{\exp[-2\pi jt(f - f_o)]/[-2\pi j(f - f_o)]$$

$$- \exp[-2\pi jt(f + f_o)]/[-2\pi j(f + f_o)]\}\Big|_{-N/(4f_o)}^{N/(4f_o)}$$

$$= (k^2C_s\Delta xf_o)^{1/2}\ (-j2f_o)\ \{\sin[\pi N(f - f_o)/(2f_o)]/[\pi(f - f_o)]$$

$$- \sin[\pi N(f + f_o)/(2f_o)]/[\pi(f + f_o)]\}$$

$$= -jN(k^2C_s\Delta xf_o)^{1/2}\ \{\mathrm{sinc}[N(f - f_o)/(2f_o)]$$

$$- \mathrm{sinc}[N(f + f_o)/(2f_o)]\} \qquad (1.5.3)$$

where sinc u = sin(πu)/(πu)

For frequencies close to f_o, equation (1.5.3) becomes

$$H(f) \simeq -jN(k^2C_s\Delta xf_o)^{1/2}\ \mathrm{sinc}[N(f - f_o)/(2f_o)] \qquad (1.5.4)$$

Thus, for an unapodized IDT, the frequency response is simply the well-known sinc function response with centre frequency f_o and bandwidth $4f_o/N$ (to the first zeroes). The magnitude of the response is determined by finger number, among other factors. The sidelobe suppression of the sinc function is not large, approximately 13.3 dB, which accounts for the prevalent use of apodization as discussed in Section 1.4.

1.5.3 Frequency Response of SAW Filter

The SAW filter system consists of three distinct series components: the input transducer, the acoustic delay line, and the output transducer. The frequency response of any linear system is the product of the frequency responses of its series components. The response of the input transducer was derived in the last section; the response of an identical output transducer can be shown to be[21]

$$H_o(f) = H_i^*(f) \tag{1.5.5}$$

The action of the delay line, in the absence of any attenuation, is simply to produce a linear phase shift with frequency, since the centre-to-centre distance of the two transducers, ℓ, is fixed. Thus,

$$H_{DL}(f) = \exp(-2\pi j f \ell / v_a) \tag{1.5.6}$$

where v_a is the acoustic velocity.

The system response, then, is

$$\begin{aligned} H_T(f) &= H_i(f)\, H_{DL}(f)\, H_o(f) \\ &= |H_i(f)|^2\, H_{DL}(f) \\ &= N^2 k^2 C_s \Delta x f_o\, \mathrm{sinc}^2[N(f - f_o)/(2f_o)]\, \exp(-2\pi j f \ell / v_a) \end{aligned} \tag{1.5.7}$$

The 3dB bandwidth of this response is $4f_o/(\pi N)$, with a sideband suppression of $\simeq$ 26.5 dB. Also, the linear phase sought by Kalman as described in Section 1.1 is quite evident here.

1.6 Network Analysis

The frequency response of the SAW filter alone is not the response of the complete SAW device. Consideration of losses, load, and distributed reactance are necessary to establish the operating characteristics of the device. Losses in the system include acoustic propagation loss, the finite resistance of electrodes and connecting wires, and dipole radiation of the electrode array. The choice of load influences the loss due to mismatch as does the source impedance value. Distributed reactance arises primarily in interelectrode capacitance, but terms due to connecting wire and bus bar capacitance and inductance are present; similarly, the acoustic and electromagnetic radiation of the array induces some reactive energy storage.

The general procedure used here in determining the equivalent circuit of the input transducer, for instance, is to lump source impedance, resistive losses and distributed reactance into an impedance in series with the parallel combination of electrode capacitance, conductance and susceptance. Loss due to dipole radiation is not considered further here but treated in Section 3.3.

The effect of the IDT may be represented by four passive elements, namely:

1. Radiation Conductance, G_a

2. Radiation Susceptance, B_a

3. Electrode Capacitance, C_T

4. Electrode Resistance, R_e

The fact that all these elements, apart from electrode resistance, R_e, are admittance terms appears to stem from the widespread use of lithium niobate ($LiNbO_3$) substrates in SAW design. Milsom et al.[12] shows that the crossfield model most appropriate for $LiNbO_3$ based devices leads to a current-driven equivalent circuit. Thus, admittance terms are conventionally used to describe filter characteristics. These elements will be studied separately, then the circuit analysis will be presented.

1.6.1 Radiation Conductance

Hartmann shows that for a lossless transducer, the radiation conductance is given by

$$G_a(f) = 2|H(f)|^2 \qquad (1.6.1)$$

The lossless restriction can be taken to mean negligible dipole radiation, since other losses will be lumped into the source/load impedance. The conductance is therefore given by

$$G_a(f) = 2N^2k^2C_s\Delta x f_o \mathrm{sinc}^2[N(f - f_o)/(2f_o)] \qquad (1.6.2)$$

1.6.2 Radiation Susceptance

Hartmann also shows that the radiation susceptance is related to the radiation conductance through the Hilbert transform:

$$B_a(f) = (1/\pi) \int_{-\infty}^{\infty} [G_a(f')/(f' - f)]\, df'$$

$$= 4N^2k^2C_s\Delta x f_o[(\sin\theta - \theta)/\theta^2] \qquad (1.6.3)$$

where $\theta = \pi N(f - f_o)/f_o$

For frequencies close to the synchronous frequency, radiation susceptance is usually taken to be negligible.

1.6.3 Electrode Capacitance

The capacitance of the IDT is simply

$$C_T = NC_s\Delta x/2 \qquad (1.6.4)$$

since there are N/2 pairs of electrodes in parallel.

As mentioned previously, electrode capacitance is generally the dominant reactance and, in fact, is generally the dominant impedance.

1.6.4 Electrode Resistance

The formula for resistance is

$$R = \rho L/A \qquad (1.6.5)$$

where ρ is the resistivity of the conductor, L, its length, and A, its cross-sectional area.

This formula can be used to derive the following expression for electrode resistance at a metallization ratio of $\eta = 1/2$:

$$R_e = 4\rho\Delta x/(\lambda_o t) \qquad (1.6.6)$$

where t is the thickness of the conducting layer and λ_o, the synchronous wavelength.

For N+1 electrodes

$$[R_e]_T = R_e/(N+1) \qquad (1.6.7)$$

Electrode resistance is usually assumed negligible and does not appear explicitly in the circuit analysis to follow. Rather, it can be

incorporated, when necessary, along with other series losses or stray reactances, in the source impedance term.

1.6.5 Equivalent Circuit

The elements considered in the preceding sections can be combined with a Thevenin generator and source impedance to yield the equivalent circuits shown in Figure 1.5. Circuit a) is used when loss terms and stray reactance terms are explicitly included in the analysis. As mentioned in Section 1.6.4, these terms could be included in the source impedance term with an appropriate change in the generator voltage. Circuit b) is used when the losses and stray reactance terms are negligible. A compromise used in this thesis is to use circuit b) but including a stray capacitance term with the static capacitance C_T. Straightforward circuit analysis of circuit b) gives the voltage across the transducer as

$$V_T = V_i/\{1 + Z_s[G_a + j(B_a + \omega C_T]\} \qquad (1.6.8)$$

The acoustic power output of the transducer is represented by the radiation conductance, G_a. This power can be written as

$$P_a = |V_i|^2 \, G_a/\{(1 + G_a Z_s)^2 + [Z_s(B_a + \omega C_T)]^2\} \qquad (1.6.9)$$

assuming Z_s real.

Since insertion loss* is a major consideration in filter design, the output power of the transducer relative to the maximum possible

---

* The term insertion loss used here is sometimes referred to as effective transmission loss; that is, the insertion loss is the difference (in dB) between power transmitted to the load and the maximum power attainable from the generator.

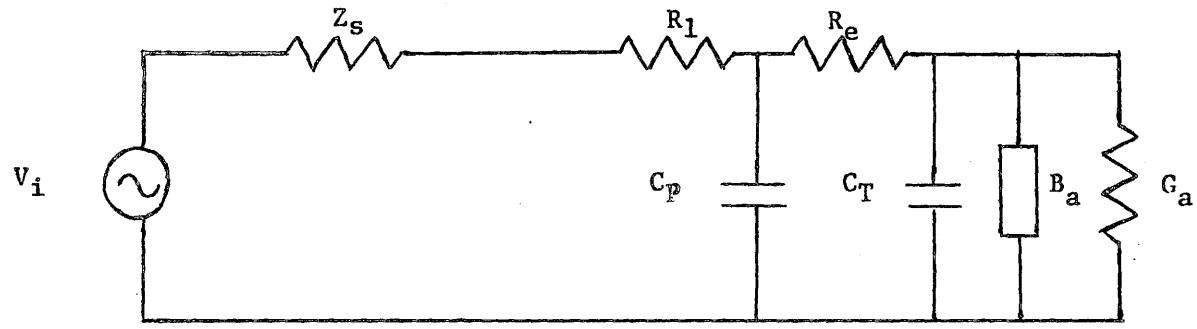

Circuit a) for large losses

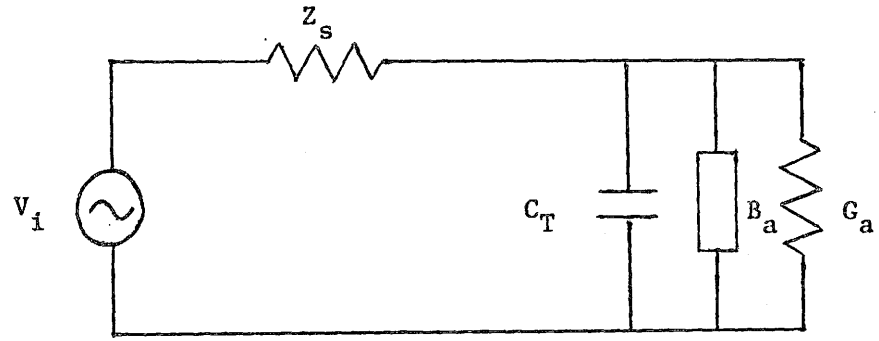

Circuit b) for small losses

Figure 1.5 Equivalent Circuits for Input Transducer

power transfer from the Thevenin driver is needed. The maximum power transfer occurs under matched conditions; that is

$$P_{max} = |V_i|^2/(4Z_s) \qquad (1.6.10)$$

Thus, the acoustic power output relative to this maximum which reaches the output transducer is

$$p = 2G_aZ_s/\{(1 + G_aZ_s)^2 + [Z_s(B_a + \omega C_T)]^2\} \qquad (1.6.11)$$

where a factor of 1/2 has been applied to account for the bidirectionality of the transducer. Acoustic propagation losses have been neglected in this analysis.

By symmetry and reciprocity, assuming identical input and output transducer configurations, the same power transfer coefficient defined by equation (1.6.11) holds for the output transducer.

The insertion loss of the device, under these assumptions, is given by

$$IL = 20 \log |p| \text{ (dB)} \qquad (1.6.12)$$

If loss mechanisms are present, their effect can be added (in dB) to the insertion loss just defined provided they do not seriously affect the operating characteristics established by the circuit elements.

From equation (1.6.8), the phase response of the filter in the absence of distortion can be found again assuming identical input and output transducers. The effects of distortion are covered in Chapter 3.

The phase response is given by twice the arc tangent of the ratio of the real and imaginary parts of the output voltage. Any phase characteristics of the input signal would add to this circuit phase factor. Thus,

$$\phi_c(f) = -2\tan^{-1}[Z_s(B_a + \omega C_T)/(1 + G_a Z_s)] \qquad (1.6.13)$$

Finally the input impedance is given directly from Figure 1.5b) as

$$Z_i = [G_a + j(B_a + \omega C_T)]^{-1} \qquad (1.6.14)$$

By symmetry the output impedance is

$$Z_o = Z_i \qquad (1.6.15)$$

1.7 Characteristics of SAW Filters

Wideband filters are generally specified by eight parameters.

1. Centre Frequency: The centre frequency of the desired frequency response serves to locate that response in the frequency domain.
2. Bandwidth: The bandwidth of the filter determines the range of the passband or that range of frequencies which are not attenuated by the filter. The bandwidth can be specified as a percentage of the centre frequency or as the actual width of the "passband".
3. Insertion Loss: The power transmitted by the filter relative to that delivered by a perfectly matched system is called the insertion loss. It is usually stated in dB and can be given as a frequency characteristic over the entire band or as the insertion loss at the centre frequency.
4. Input/Output Impedance: Input and output impedance are important parameters since they reflect the compatibility of the filter with existing devices. However, specification of the insertion loss usually predetermines these parameters and vice versa.
5. Group Delay: The measure of phase linearity with frequency is

called the group delay. Ideally the group delay should be constant with frequency. The delay can be specified as the nominal delay at the centre frequency or as a range of allowable deviation from linearity over the band. Group delay is defined as:

$$T(f) = -\frac{1}{2\pi}\frac{d\phi}{df} \qquad (1.7.1)$$

where ϕ is the phase characteristic of the filter response

$$\phi(f) = \tan^{-1}\{Im[H(f)]/Re[H(f)]\} \qquad (1.7.2)$$

6. Sideband Suppression: Signal-to-noise ratio is affected by the presence of large sidebands, thus suppression of these sidebands is also an important consideration. Suppression is usually stated in dB.

7. Transition Bandwidth: The rate at which the frequency characteristic rolls off outside the passband is given by the quotient of the sideband suppression and the transition bandwidth. The transition bandwidth, in effect, determines the shape of the filter response.

8. Passband Effects: The ideal passband is completely flat. The extent of deviations from this state of flatness are, therefore, of interest. These deviations can take the form of amplitude and phase ripple or some asymmetry in the band.

The determination of these parameters in conventional SAW filters will now be examined.

1. Centre Frequency: As shown in Section 1.4, the centre frequency

of the conventional SAW filter is determined by the spacing of the electrodes.

2. Bandwidth: The bandwidth of SAW filters is inversely proportional to the number of fingers as discussed in Section 1.5.3. This is perhaps the greatest limitation of conventional SAW filters. To achieve a wideband the number of fingers must be kept low. Consequently, the input impedance is low and the filter becomes very hard to match. The electrode resistance also increases with decreasing finger number which constitutes another loss in the system.

3. Insertion Loss: The insertion loss of SAW filters was given in Section 1.6.5. By combining equations (1.6.11) and (1.6.12) for small G_a and B_a:

$$IL \simeq 20 \log |2G_a Z_s/[1 + (\omega C_T Z_s)^2]| \qquad (1.7.3)$$

Thus the insertion loss is linearly related to the log of the admittance. At the centre frequency, this admittance is equal to

$$G_a = 2N^2 k^2 C_s \Delta x f_o \qquad (1.7.4)$$

as given by equation (1.6.2).

Finger number, N, is related to the percentage bandwidth, BW, by

$$N \simeq 4/(\pi \text{ BW}) \qquad (1.7.5)$$

Combining equations (1.7.3), (1.7.4) and (1.7.5), it can be seen that insertion loss is related to 40 log BW.

4. Input/Output Impedance: For small G_a and B_a the input/output impedance is determined predominantly by the electrode

capacitance. The aperture in equation (1.6.4) can be adjusted to give

$$C_T = |2\pi f_o Z_s|^{-1} \tag{1.7.6}$$

In terms of aperture Δx, this can be written

$$\Delta x = |\pi N C_s f_o Z_s|^{-1} \tag{1.7.7}$$

Thus for small finger number, N, the aperture for a matched filter must be large. This places a strain on the fabrication technique; high resolution must be established over a large area. Actually, in practical filters, some degree of mismatch is deliberately imposed to reduce distortion effects as discussed in Chapter 3. The trade-off in terms of insertion loss should be evident at this point.

5. Group Delay: For a transducer symmetrical about its centre finger, the phase is nominally linear as shown in Section 1.3. Distortion mechanisms and circuit effects can cause deviations from linear phase, however. In fact, attaining constant group delay is usually the most difficult aspect of SAW filter design due to the tight constraints evidenced in Figure 1.1. For instance, the group delay for a 50% bandwidth filter must be kept within 5 ns of its value at the centre frequency over better than 80% of the band. This translates to a phase shift of less than 60 degrees over the same band. Various methods are used for reducing distortion, the most useful of which are given in Chapter 3. However, these methods usually require an increase in insertion loss and/or design complexity.

6. Sideband Suppression: The improvement of the elementary SAW filter sideband suppresion, given in Section 1.5.3, through the use of windowing or apodization was touched on in Section 1.4. The improvement is offset, however, by the increase in diffraction losses resulting from the decreased apertures of apodized finger pairs. Also, there is a lack of flexibility in the sense that each finger influences two finger pairs not just one. Apodization is treated more fully in Tancrell[21] or Hartmann[6].

7. Transition Bandwidth: As with sideband suppression, the reduction of transition bandwidth from the elementary SAW filter characteristic is accomplished through apodization. The reader is referred to Hartmann[6] for a more complete discussion. The shortcomings of apodization were mentioned in the last paragraph.

8. Passband Ripple: Ripple, due primarily to distortion mechanisms discussed in Chapter 3, degrades the performance of all SAW filters. Minimization of these distorting elements is also covered in Chapter 3. Another passband effect which becomes noticeable at large bandwidth is the sloping of the response rather than the desired flatband response. This effect is mostly due to capacitance which bleeds off the higher frequencies resulting in a decreased high frequency response.

1.8 Thesis Proposal

The limitations of conventional SAW filters have been outlined in

Section 1.7. To summarize, the major difficulties are:

1. The coupling of bandwidth with number of fingers, results in practical limitations on the ability to match a device with very few fingers.
2. The relation between insertion loss and bandwidth also imposes limitations on the maximum allowable bandwidth.
3. The presence of distortion destroys the inherent linear phase of the SAW filter. Methods for reducing distortion usually impose constraints on insertion loss or design complexity.
4. Apodized transducers, used to improve transition bandwidth and sideband suppression, are not completely flexible and introduce distortion in the form of diffraction into the system.
5. For very wideband filters, circuit effects tend to cause asymmetric filter response predominantly due to static or stray capacitance.

In this thesis, a two-part scheme is proposed which divides the difficulties listed above into two categories. First, the effects due to circuit elements and the restricted nature of the conventional SAW filter are resolved by the introduction of a new filter design. This new design draws heavily on the ability to fabricate photomasks with fingers of arbitrary curvature. However, the proliferation of computer-controlled draughting tables in the past few years stands in favour of this approach.

By using curved fingers, the coupling between bandwidth and

finger number is removed. Secondly, finger curvature can be modified to compensate for any detrimental circuit effects. Finally, the finger number controls, to first order, the transition width and the inherent passband ripple of transversal filters.

It should be mentioned that the curved finger transducer will still have a relatively high insertion loss within a few dB of that corresponding to the maxumum allowable bandwidth in conventional SAW transducers. However, the added flexibility they offer should produce a competitive product.

The second part of the two-part scheme is the minimization of distortion effects by judicious choice of SAW parameters such as transducer separation and acoustic aperture, or through a variety of other methods covered in Chapter 3.

Care in packaging is one of the most fundamental ways of improving filter performance; the elimination of unnecessary stray capacitance and excessive lead lengths, combined with intelligent use of antireflection materials, topped off with a good hermetic seal will enormously reduce the amount of compensation otherwise necessary in the design of a working filter.

In the following chapters, these two courses of filter design will be studied consecutively. The fabrication methods used in constructing devices are described in Chapter 4. The characteristics of these devices are presented in Chapter 5 for the purpose of illustrating the theory developed in the earlier chapters.

CHAPTER 2

CURVED FINGER TRANSDUCER THEORY

2.1 Curved Finger Transducers

The curved finger transducer family is that group of transducers for which the synchronous frequency is a function of position along the aperture as shown in Figure 2.1. This family includes the limiting cases of straight (conventional) finger and slanted finger transducers.

The action of these transducers is to spatially separate frequency components of the applied field. Each finger in the transducer sets up acoustic waves in synchronism with the excitation. However, the cumulative effect of the electrode separation distance along a thin strip perpendicular to the length of the finger is to enhance the synchronous frequency and suppress all frequencies not harmonic with the synchronous frequency. By varying the curvature of the fingers, one can change the slope of the composite transfer function of the SAW filter, to account for any capacitive or inductive effects, or simply to produce a given slope on the passband.

2.2 Frequency Response of Curved Finger Transducer

2.2.1 General Derivation

The frequency response of a transducer with finger curvature is based on the sum of the responses of elementary straight finger transducers of width Δx, and synchronous frequency $f_o(x)$ as discussed in

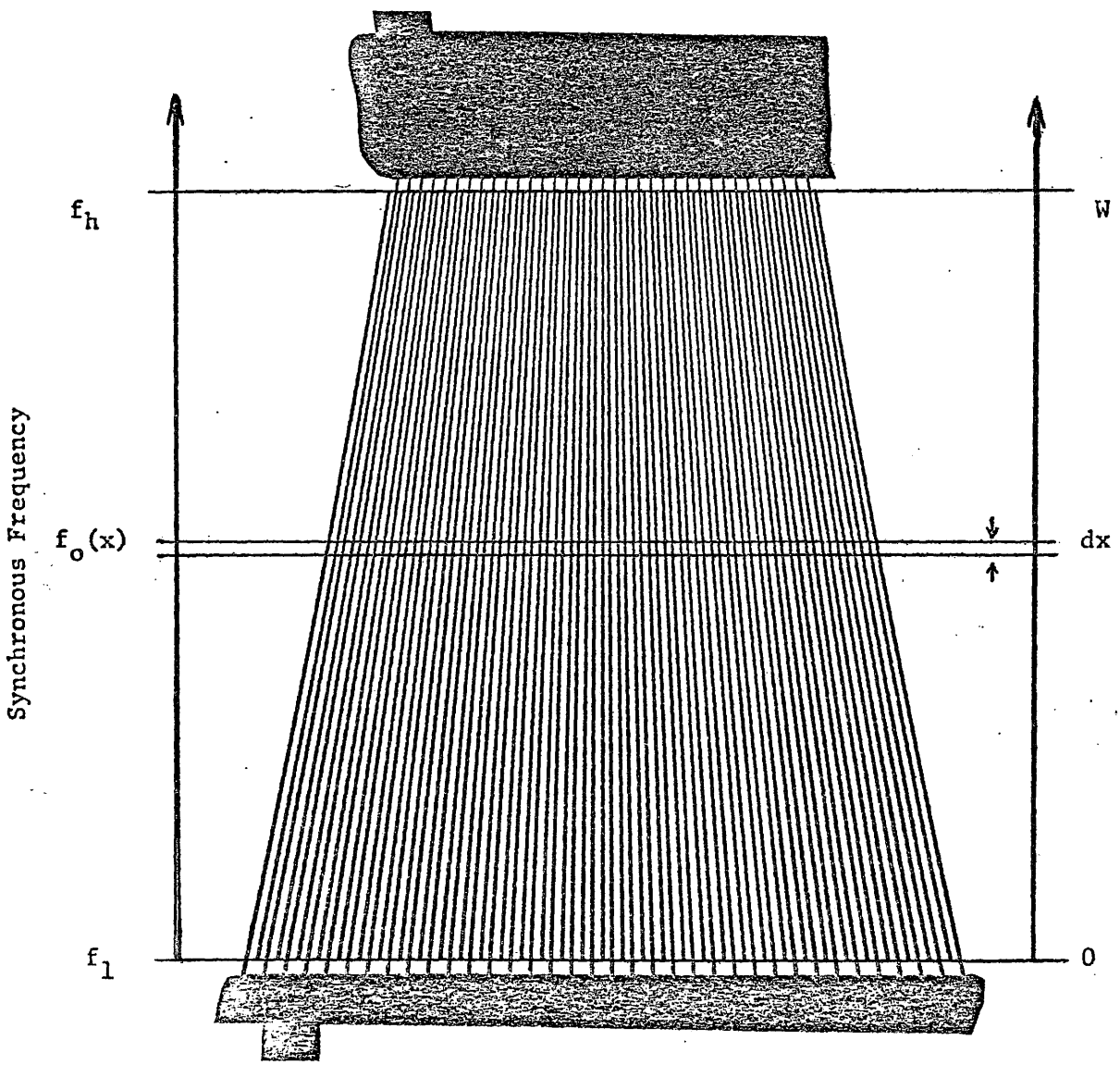

Figure 2.1 Curved Finger Transducer Geometry

Section 1.5. Frequency selectivity is a measure of the independence of each elementary strip and is determined by the number of fingers; that is, the larger the number of fingers, the narrower the bandwidth of an individual strip. For the purpose of this derivation, all strips are assumed to have N+1 fingers.

Combining the elementary strips over a range from lower cutoff frequency, f_ℓ, to upper cutoff frequency, f_h, the transfer function of the composite filter is, in the limit of infinitismal Δx:

$$H_c(f) = \int_{x(f_\ell)}^{x(f_h)} N^2k^2C_s\, f_o\, \mathrm{sinc}^2[N(f-f_o)/(2f_o)]\exp(-2\pi jf\ell/v_a)dx \qquad (2.2.1)$$

where $f_o = f_o(x)$

This can also be written as

$$H_c(f) = \int_{f_\ell}^{f_h} N^2k^2C_s\, f_o\, \mathrm{sinc}^2[N(f-f_o)/2f_o)]\exp(-2\pi jf\ell/v_a)x'(f_o)df_o \qquad (2.2.2)$$

where $x'(f_o) = \dfrac{dx}{df_o}$

For large N, the sinc( ) function can be associated with the terms of a delta function sequence[1]:

$$\delta_N(\partial) = \sin(N\partial)/(\pi\partial) \qquad (2.2.3)$$

which has the properties:

1. $$\int_{-\infty}^{\infty} \delta_N(\partial)d\partial = 1 \qquad (2.2.4)$$

$$2. \qquad \lim_{N\to\infty} \int_A^B \delta_N(\partial-\partial_i)\, f(\partial)\,d\partial = f(\partial_i) \quad A \leq \partial_i \leq B \qquad (2.2.5)$$

$$= 0 \qquad \text{else}$$

$$3. \qquad \delta_N[\partial(f_o)] = \sum_{i=1}^{p} \delta_N(f_o-f_i)/|\partial'(f_i)| \qquad (2.2.6)$$

where f_i is one of p simple zeroes of ∂.

Thus, sinc( ) in equation (2.2.2) can be written

$$\text{sinc}(\ ) = \sin[\pi(\ )]/[\pi(\ )]$$

$$= (\pi/N)\,\delta_N[(\pi/N)(\ )] \qquad (2.2.7)$$

which for $(\ ) = N(f-f_o)/(2f_o)$ becomes

$$\delta_N[(\pi/N)(\ )] = \delta_N[\pi(f-f_o)/(2f_o)]$$

$$= (2f_o/\pi)\delta_N(f-f_o) \qquad (2.2.8)$$

by property (2.2.6)

Substitution of (2.2.8) and (2.2.7) into (2.2.2) yields

$$H_c(f) = 2N\,k^2C_s \exp(-2\pi jf\ell/v_a) \int_{f_\ell}^{f_h} f_o^{\,2} \sin(\ )\,\delta_N(f-f_o)x'(f_o)df_o$$

$$\simeq 2N\,k^2C_s \exp(-2\pi jf\ell/v_a)\, f^2x'(f) \quad f_\ell \leq f \leq f_h \qquad (2.2.9)$$

$$\simeq 0 \qquad \text{else}$$

in the limit of large N.

2.2.2 Slanted Finger Transducer Response

For a slanted finger transducer, the distance x along the aperture varies linearly with synchronous wavelength. Using the convention of Section 2.2.1, for a transducer of total aperture W:

$$x = W[(f_o^{-1} - f_\ell^{-1})/(f_h^{-1} - f_\ell^{-1})]$$
$$= (Wf_h f_\ell/\Delta f)(f_\ell^{-1} - f_o^{-1}) \qquad (2.2.10)$$

where $\Delta f = f_h - f_\ell$

Then $x'(f_o) = (W f_h f_\ell/\Delta f) f_o^{-2}$ (2.2.11)

and

$$H_s(f) \simeq 2N k^2 C_s \exp(-2\pi j f\ell/v_a) W f_h f_\ell/\Delta f \quad f_\ell \leq f \leq f_h \qquad (2.2.12)$$
$$\simeq 0 \qquad \text{else}$$

This, in fact, is equal to the ideal bandpass frequency response with flat passband response and linear phase across the bandwidth, Δf. It must be emphasized that this result depends on a large finger number. Thus, when Campbell et al.[3] found a sloping band pass response from a slanted finger transducer, the effect was due to factors external to the transducer frequency response. In fact, it will be shown in the following sections that the sloping response is, in fact, predominantly due to the associated finger capacitance. Before this, however, the effect of alternate finger curvatures will be investigated.

2.2.3 Other Finger Curvatures

If the synchronous frequency is made to vary with the power p along the aperture coordinate x, then

$$x = W(f_o^p - f_\ell^p)/(f_h^p - f_\ell^p) \qquad p \neq 0,\ p \in R \qquad (2.2.13)$$

Then $x'(f_o) = [pW/(f_h^p - f_\ell^p)] f_o^{p-1}$

and

$$H_c(f) \simeq 2Nk^2 C_s \exp(-2\pi j f\ell/v_a) [pW/(f_h^p - f_\ell^p)] f^{p+1} \quad f_\ell \leq f \leq f_h \qquad (2.2.14)$$
$$\simeq 0 \qquad \text{else}$$

The slope of the passband due to the effect of finger curvature can be calculated with respect to power p as follows:

$$\text{Slope} = 20 \log|H_c(f_h)/H_c(f_\ell)|$$

$$= 20\,(p+1) \log|f_h/f_\ell| \qquad (2.2.15)$$

The results for selected values of p are tabulated below, for a 50% bandwidth filter:

TABLE 2.1

Variation of Passband Slope with Curve Parameter p

p	Slope (dB)
1.0	8.87
0.5	6.66
-0.5	2.22
-1.0	0.00
-1.5	-2.22
-2.0	-4.44

2.3 Network Analysis of Curved Finger SAW Device

Following the analysis of Section 1.6, the pertinent passive elements corresponding to curved finger transducers and the resulting network parameters will now be determined.

2.3.1 Curved Electrode Conductance

The conductance of a lossless curved electrode IDT is given, as in Section 1.6.1, by

$$G_{ac}(f) = 2|H(f)|^2$$
$$\simeq 4\, Nk^2C_s\, f^2\, x'(f) \qquad f_\ell \leq f \leq f_h$$
$$\simeq 0 \qquad \text{else} \tag{2.3.1}$$

For slanted fingers this reduces to

$$G_{as}(f) \simeq 4\, Nk^2C_s\, W\, f_h f_\ell/\Delta f \qquad f_\ell \leq f \leq f_h$$
$$\simeq 0 \qquad \text{else} \tag{2.3.2}$$

Therefore, the conductance of slanted finger transducers is independent of frequency within the band.

2.3.2 Curved Electrode Susceptance

Once the curved electrode conductance is determined, the susceptance can be found using the Hilbert transform:

$$B_{ac}(f) = (1/\pi) \int_{-\infty}^{\infty} [G_a(f')/(f' - f)]df'$$

$$\simeq (4Nk^2C_s/\pi) \int_{f_\ell}^{f_h} [(f')^2\, x'(f')/(f' - f)]df' \tag{2.3.3}$$

For slanted fingers, equation (2.3.3) reduces to

$$B_{as}(f) \simeq 4\, Nk^2C_s\, W\, f_h f_\ell/(\pi\Delta f)\, \ln|(f_h - f)/(f - f_\ell)|$$
$$= (1/\pi)G_{as}\, \ln|(f_h - f)/(f - f_\ell)| \tag{2.3.4}$$

Thus, $B_{as}(f)$ is bounded by

$$|B_{as}(f)| \leq \varepsilon\, G_{as} \text{ for } |f - f_c| \leq (\Delta f/2)\, \sinh(\pi\varepsilon/2) \tag{2.3.5}$$

where f_c is the centre frequency of operation. Since the susceptance is small relative to the capacitance except at the band limits it will

generally be ignored in circuit analysis.

2.3.3 Curved Electrode Capacitance

The capacitance of a curved finger transducer is given by

$$C_T = (1/2) \int_0^W NC_s dx$$

$$= 1/2\ NC_s W \qquad (2.3.6)$$

independent of actual finger curvature. Naturally this is only an approximation, but, in the absence of more advanced analysis, will suffice.

2.3.4 Curved Electrode Resistance

Following Section 1.6.5, the curved electrode resistance is given by

$$R_e = \int_o^W [4\rho/(\lambda_o(x)t)]dx$$

$$= (4\rho/v_a t) \int_{f_\ell}^{f_h} f_o\ x'(f_o)df_o \qquad (2.3.7)$$

For slanted finger transducers, equation (2.3.7) becomes

$$R_{es} = (4\rho\ W\ f_h f_\ell / v_a t\ \Delta f)\ \ln|f_h/f_\ell| \qquad (2.3.8)$$

For 50% bandwidth, the reduces to

$$R_{es} = 3.83\ (\rho W/\lambda_c t) \qquad (2.3.9)$$

where λ_c is the wavelength corresponding to the centre frequency.

The resistance of N+1 electrodes in parallel is, again

$$[R_{ec}]_T = R_{ec}/(N+1) \qquad (2.3.10)$$

2.4 Network Parameters

Using the equivalent circuit of Figure 1.5, the input impedance, output impedance, insertion loss and group delay of the curved electrode transducer may be determined, following the procedure of Section 1.6.5.

2.4.1 Input/Output Impedance of Curved Finger Transducer

From equations (1.6.14) and (1.6.15) the input and output impedance of curved finger transducers may be written as

$$Z_i = Z_o = [G_a + j(B_a + \omega C_T)]^{-1} \qquad (2.4.1)$$

Using the appropriate parameters from the last sections.

For slanted fingers near the centre of the band, where BW is the percentage bandwidth

$$Z_{is}^{-1} = Z_{os}^{-1} = (\omega_c C_T)\ [4k^2(1 - BW^2/4)/(\pi BW) + jf/f_c] \qquad (2.4.2)$$

For a 50% bandwidth filter on $LiNbO_3$, this reduces to

$$Z_{is}^{-1} = Z_{os}^{-1} \simeq \omega_c C_T\ [.1098 + jf/f_c] \qquad (2.4.3)$$

2.4.2 Insertion Loss of Curved Finger Transducer

If the insertion loss over the entire range of the filter is desired, then calculation of $B_a(f)$ must be performed, since it becomes sizable near the band limits. Once this calculation has been performed it is a simple matter to substitute into equations (1.6.11) and (1.6.12) to calculate the insertion loss. Naturally the actual behaviour of $B_a(f)$ at the band limits requires a more advanced calculation of $G_a(f)$

than that afforded by equation (2.3.1). In other words, the reality of finite N must be dealt with. At this point it is probably simpler to go to a numerical solution. For $B_a(f)$ well within the band, however, the assumption of small $B_a(f)$ is not unreasonable.

2.4.3 Group Delay of Curved Finger Transducer

The phase of the transducer circuit in the absence of distortion is the sum of any intrinsic phase associated with the input signal and the circuit phase defined in equation (1.6.13).

If $B_a(f)$ can be considered negligible and the system matched such that $Z_s = (\omega_c C_T)^{-1}$, then

$$\phi_c(f) \simeq -2 \tan^{-1}\{f/[f_c(1 + Z_s G_a)]\} \qquad (2.4.4)$$

The group delay, as defined by equation (1.7.1), is then

$$T_c(f) \simeq (\pi f_c)^{-1} (1 + Z_s G_a)/[(1 + Z_s G_a)^2 + (f/f_c)^2] \qquad (2.4.5)$$

The change in group delay over the band is well within the constraints given in Figure 1.1. For instance, with f_c = 70 MHz and a bandwidth of 50%, the change in group delay over the entire band to less than 1.14 ns for all values of G_a. The allowed variation is 15 ns. Distortion, covered in Chapter 3, places a more severe restriction on group delay than circuit factors. As before, for a complete analysis the effect of $B_a(f)$ must be considered. The direction of effort, at least in terms of group delay, obviously must be towards minimizing the distortion effects on group delay, for the time being.

2.5 Practical Limitations

The accuracy to which a given finger curvature can be produced is limited by the initial mask fabrication process. In the system used here, the finger curve must be composed of piecewise linear segments. Since each linear segment requires a finite amount of memory to store the pertinent information, there is a limitation on the degree to which a given curvature can be achieved. A further consideration is the time needed to produce the mask which, obviously, increases as the complexity of the mask increases.

If this ultimate limitation is to be taken into consideration, the analysis must provide for a superposition of slanted finger transducer responses with adjacent centre frequencies. For the purpose of this thesis, ten strips were found to suffice for nonslanted finger structures.

The problem with finite N has been addressed somewhat offhandedly in Sections 2.2.2 and 2.4.2. The most important practical result of using a finite impulse response filter is the introduction of ripples in the passband. Naturally, this inherent ripple should be minimized to yield the flattest passband response. Since the overall SAW filter frequency response is the product of the input and output transducer frequency responses, the worst case for inherent ripple is with identical transducers. For this case, the overall ripple will double (in dB) from that of the individual transducer ripple amplitude. The simplest way of reducing the ripple then is to use dissimilar transducers in terms of finger number. In this way, the ripple in each

transducer response will be slightly out of phase producing "destructive interference" and an averaging effect over the passband. The optimal values for finger number can be found by computer simulation, trial and error or possibly an analytical solution can be found in the domain of transversal filters.

CHAPTER 3

DISTORTION IN SAW FILTERS

3.1 General

As explained in Chapter 1, the design of SAW filters in this thesis, is divided into two areas. The first, the design of the SAW filter to provide a desired (nominal) characteristic through the use of finger curvature, was covered in Chapter 2. The second, the minimization of perturbations of this nominal characteristic, is the subject of this chapter.

The main sources of distortion in SAW filters are:

1. Reflections
2. Electromagnetic feed through
3. Bulk waves

Each of these mechanisms are presented, in turn, in the following sections, along with their effect on filter performance. Methods of reducing or eliminating the effects are also considered.

It should be noted that diffraction is not treated as a major source of distortion here. The effects of diffraction are well-known and can be found in Farnell[5] or Tancrell.[21] Diffraction effects predominate when input and output transducers are separated by a distance much larger than their aperture. This is not the case for the masks considered here. Furthermore, the anisotropy of the crystals used provides an autocollimation effect. This effect is particularly

pronounced in lithium niobate ($LiNbO_3$) crystals used for all experimental filters in this work. With $LiNbO_3$, a wave may travel ten times farther before exhibiting the comparable beamspread of an isotropic medium.

Similarly, distortion due to fabrication errors is not treated here, but is covered by Bell and Clairborne[2].

3.2 Reflections

Acoustic reflections between the input and output transducers can interfere with the main beam resulting in frequency-dependent ripple in the amplitude and phase response of the filter. The period of this ripple is given by the inverse of twice the delay time between the transducers as

$$f_p = v_a/(2\ell) \tag{3.2.1}$$

where ℓ is the centre-to-centre transducer spacing. Wave reflections, in general, occur at the boundary between two media with differing characteristic impedance. An amplitude reflection coefficient can be defined as

$$r = (Z_2 - Z_1)/(Z_2 + Z_1) \tag{3.2.2}$$

where Z_1 and Z_2 are the characteristic impedances of the respective media. Due to the intimately coupled electrical and mechanical forces in the piezoelectric media, acoustic wave reflections can be due to electrical or mechanical mismatch.

The case of electrical mismatch results in regeneration of acoustic waves by a transducer. The incident waves induce a voltage

across the transducer, the magnitude of which depends on the source/load impedance. Under matched conditions a maximum of one-half the acoustic power is transferred electrically to the load. The rest of the power is reradiated in two waves which travel symmetrically away from the transducer. If a short-circuit load is applied, no voltage can be generated across the transducer, assuming perfectly conducting electrodes. Consequently, no acoustic waves are regenerated. Deliberate mismatch of the output transducer is often employed to reduce the amplitude of these reflected waves at the expense of increased insertion loss.

Acoustic mismatch can be understood as follows. The acoustic impedance of a material is given by

$$Z = \rho A v_a \tag{3.2.3}$$

where ρ, A and v_a are density, area and velocity of sound of the acoustic medium, respectively.

The reflection coefficient can be written as

$$r \simeq \frac{1}{2} \Delta Z/Z$$

$$\simeq \frac{1}{2} [\Delta v_a/v_a + \Delta A/A + \Delta\rho/\rho] \tag{3.2.4}$$

for small mismatch $Z_2 \simeq Z_1$.

Consider an interface between a free piezoelectric surface and one which has a conducting layer of thickness h and density ρ_2 as in Figure 3.1. The density of the substrate is ρ_1. The effective thickness of the substrate to surface waves is of the order of a wavelength, therefore, let this thickness in the first medium be $c_f \lambda_f$.

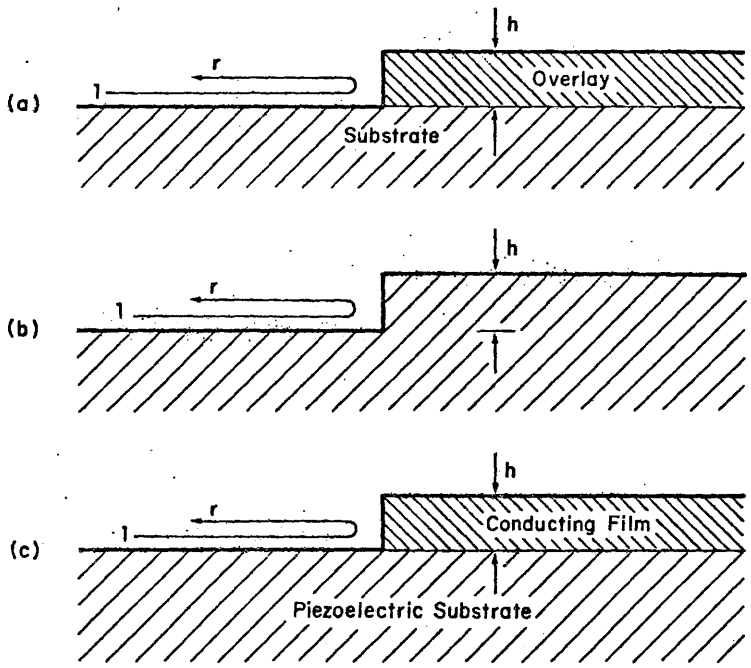

Figure 3.1 Surface perturbations that cause surface wave reflections. (*a*) General case of a thin overlay. (*b*) Vertical step. (*c*) Conducting film on a piezoelectric substrate.

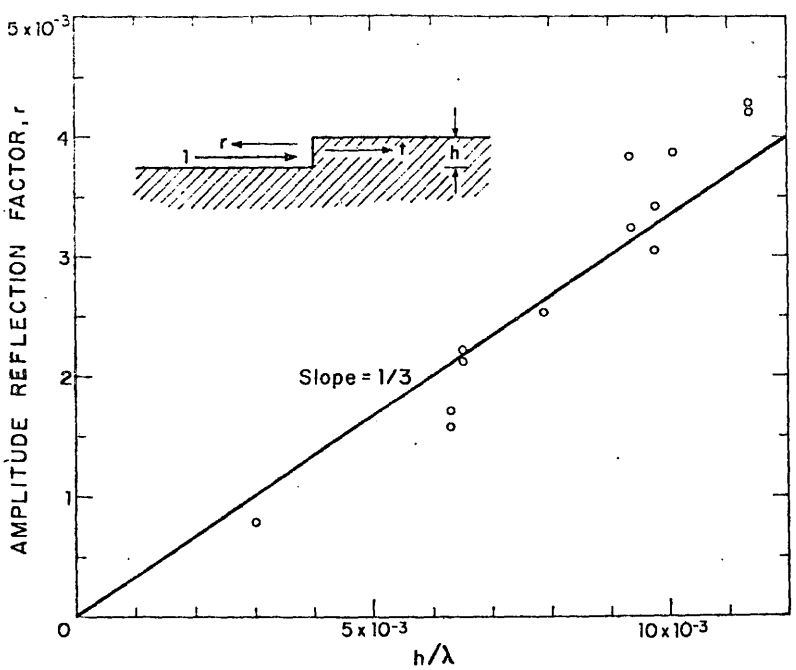

Figure 3.2 Reflectivity of a step in *YZ* $LiNbO_3$. Copyright 1973 by The Institute of Electrical and Electronic Engineers, Inc. Reprinted, with permission, from *IEEE Trans.* **MTT-21,** 1973, p. 195.

Similarly in the second medium let the effective thickness be $c_s \lambda_s$. Here, c_f and c_s are constants of order unity. The change in velocity between a free and shorted surface is given by the coupling constant of the material k^2:

$$k^2 \approx -2 (v_s - v_f)/v_f$$

From (3.2.4), the reflection coefficient can be written as

$$r \approx -k^2/4 + [\rho_2/(2 \rho_1)] h/(c_f \lambda_f) \qquad (3.2.5)$$

for $h \ll c_s \lambda_s \approx c_f \lambda_f$

Thus there are two terms which affect the reflection coefficient, the first due to the piezoelectric nature, the second due to a small step discontinuity.

Turning to practical materials, for $(h/\lambda) \leq .01$, studies have shown[22] that a step cut in a lithium niobate ($LiNbO_3$) crystal yields a reflection coefficient (see Figure 3.2)

$$r \approx .3 h/\lambda \qquad (3.2.6)$$

This is consistent with the formula derived since $\rho_2 = \rho_1$, $v_2 = v_1$, and $c_f \approx 1.5$. The value for c_f is chosen from plots of displacement amplitude versus depth[5]. The point of which the amplitude drops to e^{-1} is taken to be the effective thickness. Therefore, for an interface like the one described previously with aluminum as the conducting ($\rho_{Al} \approx 2699$ kg/m^3), the reflection coefficient is

$$r \approx - 0.0119 + .1723 h/\lambda \qquad (3.2.7)$$

for

$$k^2_{LiNbO_3} = .0476$$

$$\rho_{LiNbO_3} = 4700 \text{ kg/m}^3$$

A step in ST-quartz results in

$$r \simeq .27\ h/\lambda \tag{3.2.8}$$

From this $c_f \simeq 1.85$ and

$$r = -.0004 + .2752\ h/\lambda \tag{3.2.9}$$

for

$$k^2_{quartz} = .0016$$

$$\rho_{quartz} = 2651 \text{ kg/m}^3$$

The reflection coefficient for an array of electrodes will be a complicated function of the reflectivity of a single step (see Figure 3.3). The purpose of the preceding discussion was to introduce the important factors which effect reflectivity so that a few qualitative judgements can be drawn regarding reflection minimization. Advanced analysis of transducer reflectivity is beyond the scope of this thesis. The first observation is that the dependence of acoustic reflection on frequency is negligible for $LiNbO_3$ substrates with less than 1000 Å of aluminum deposited. For instance, a 50% bandwidth filter centred on 70 MHz with 500 Å of aluminum has a change in reflectivity of each individual step of less than 1% over the band. Reflections on quartz are a little more sensitive to frequency, due to the small coupling coefficient; in fact, it would appear that for an aluminum thickness of some 725 Å the reflection coefficient goes to zero at 70 MHz. This could be verified by further experimentation.

The reflection due to electrical mismatch will still be present.

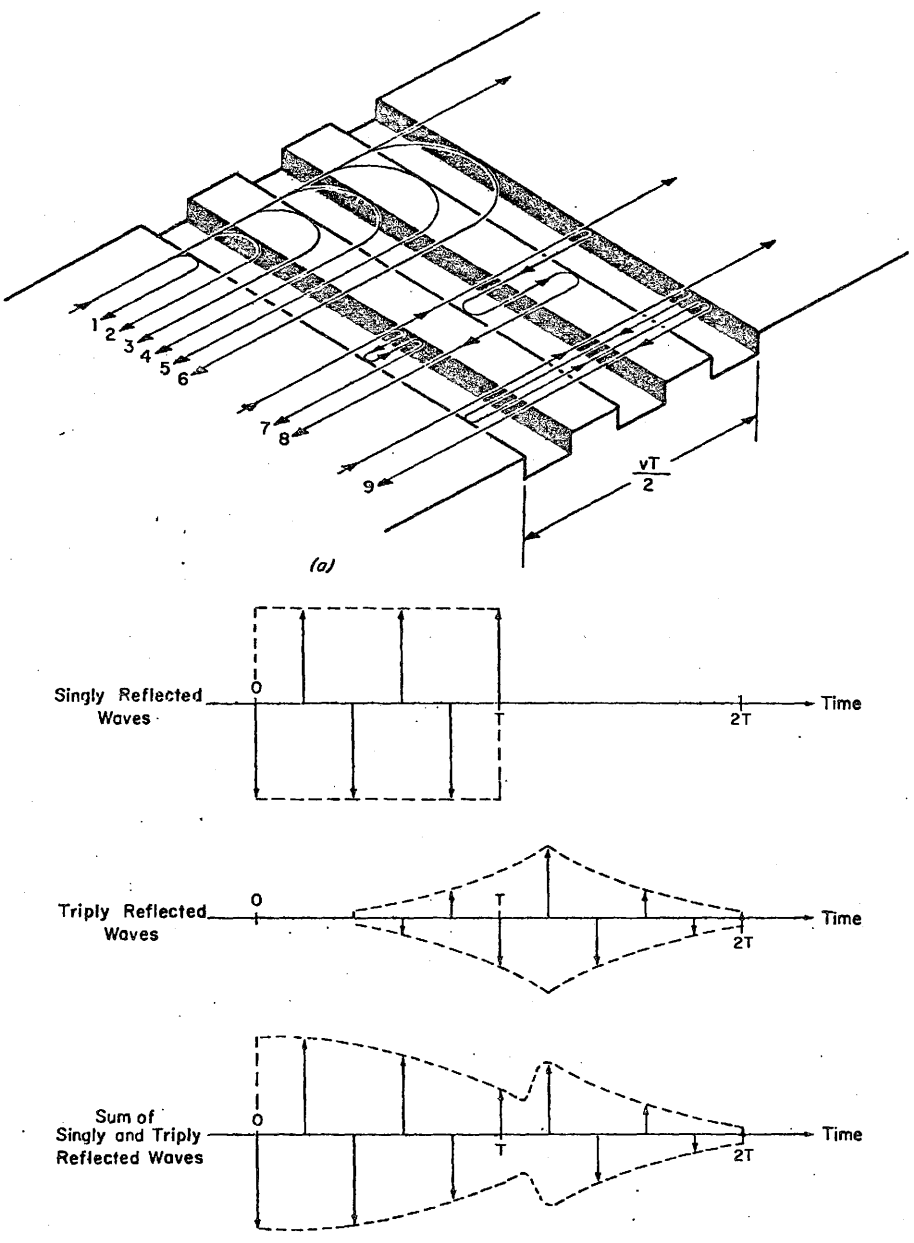

Figure 3.3 (*a*) All of the singly reflected waves and some of the triply reflected waves associated with a simple three-groove grating. (*b*) Impulse response due to singly and triply reflected waves.

The presence of an acoustic loss between the two transducers would have twice the suppression of reflected waves relative to the main signal. Thus, a trade-off between insertion loss and reflection ripple is possible. The analysis of reflected wave effect on filter response proceeds as follows.

Both input and output transducers, assumed identical, are replaced by equivalent reflectors spaced a distance ℓ apart corresponding to the former centre-to-centre transducer spacing. The reflection coefficient of each reflector will be $re^{(-j\phi_r)}$. Any propagation loss in the path between the two transducers can be incorporated in this reflection coefficient. The resultant voltage, A_T, at the output transducer will be a sum of the main signal, A_s, and all the multiply-reflected waves such that

$$\begin{aligned} A_T &= A_s\{1 + r^2\exp[-j(4\pi f\ell/v_a + 2\phi_r)] \\ &\qquad + r^4\exp[-j(8\pi f\ell/v_a + r\phi_r)] + \ldots\} \\ &= A_s/\{1 - r^2\exp[-j(4\pi f\ell/v_a + 2\phi_r)]\} \end{aligned} \qquad (3.2.10)$$

The resultant power at the output transducer is given by

$$P_T = P_A/[1 + r^4 - 2r^2\cos(4\pi f\ell/v_a + 2\phi_r)] \qquad (3.2.11)$$

Thus the input power to the output transducer has a ripple with period $f_p = v_a/(2\ell)$ as in equation (3.2.1). The peak-to-peak value of this ripple is given by

$$R_{pp} = 20\log|(1 + r^2)/(1 - r^2)| \qquad (3.2.12)$$

If the value of reflection coefficient is small, the ripple becomes sinusoidal in nature:

$$P_T \simeq P_A[1 + 2r^2\cos(4\pi f\ell/v_a + 2\phi_r)] \qquad (3.2.13)$$

This ripple is sometimes known as Triple Transit Echo (TTE), since only the first echo, which traverses the gap between the transducers three times, is strong enough to be received.

If reflective distortion is the only aberration, accurate mesurements can give values for reflection coefficient magnitude by measuring the peak to peak ripple, and reflection coefficient phase by noting the position of minima or maxima in the frequency response. The period f_p can give a reliable estimate of v_a if ℓ is known.

3.3 Electromagnetic Feedthrough

When the input and output transducers are placed too close together, the waveguiding effect of the package can cause direct electromagnetic feedthrough of the input signals. This results in amplitude and phase ripple similar to that experienced with acoustic reflections. Electromagnetic feedthrough can be distinguished from acoustic reflections, however, because the periodicity of the ripple is twice as large as shown below (see Figure 3.4). Consider the resultant voltage at the output transducer: it is the superposition of the acoustic wave generated voltage and the electromagnetic feedthrough signal. Let the amplitudes be given as A_s and A_e respectively. Then

$$A_T = A_s \exp(-2\pi f \ell/v_a) + A_e \qquad (3.3.1)$$

due to the acoustic wave's delayed signal path of length ℓ. (The phase change in the electromagnetic signal is effectively zero due to the large electromagnetic wavelength. The output signal power is

$$P_T = |A_s|^2 + |A_e|^2 + 2 A_s A_e \cos(2\pi f \ell/v_a) \qquad (3.3.2)$$

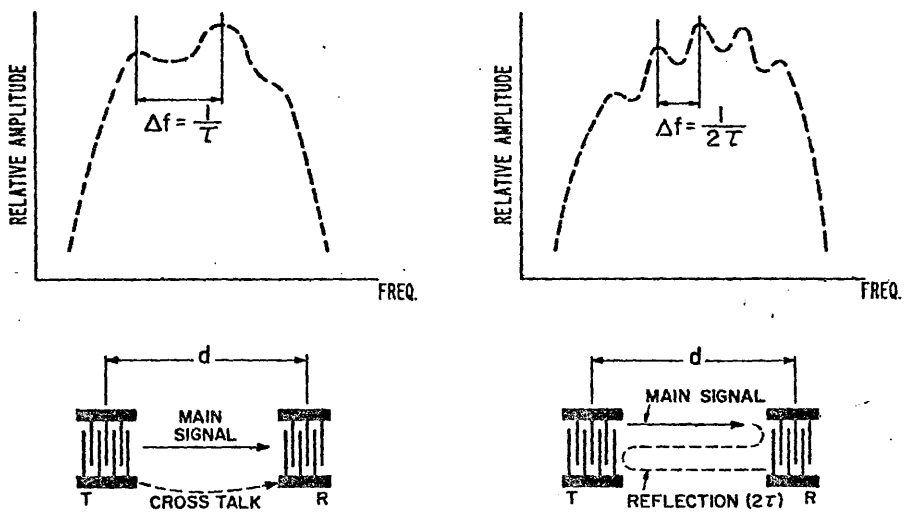

Figure 3.4 (*a*) Effect of crosstalk (direct feedthrough) on the frequency response of the filter. In the passband ripples are caused with a periodicity $\Delta f = 1/\tau$, where τ is the time for the surface waves to travel from one transducer to the other. (*b*) Effect of triple transit reflections—periodicity is $\frac{1}{2}\tau$. Copyright 1971 by The Institute of Electrical and Electronic Engineers, Inc. Reprinted, with permission, from *IEEE Trans.* **BTR-17,** 1971, p. 21.

The peak to peak ripple is given by

$$R_{pp} = 20 \log |(1+\rho)/(1-\rho)| \qquad (3.3.3)$$

where $\rho = A_e/A_s$, assuming $A_e < A_s$. By considering the guided wave to be TE_{10} mode the attenuation is given by

$$\rho = \exp(-\alpha \ell), \qquad (3.3.4)$$

where $\alpha \simeq \pi/a$, a being the cavity (box) height[20]. Thus, the larger the transducer spacing and the smaller the cavity height, the less the feedthrough signal. It seems reasonable to expect a correlation between transducer aperture and feedthrough since the larger the antenna the more microwave power emitted.

Electromagnetic feedthrough can be reduced most easily by connecting opposite sides of the input and output transducer to ground. The use of balanced transformers is also known to reduce the feedthrough signal[20]. A balanced transformer effectively positions the potential of the cavity midway between the poles of the transducer. The resultant electric field thus sums almost to zero and there is no electromagnetic feedthrough. Another technique for reduction of feedthrough involves positioning cavity-width reducing conducting elements strategically between the crystal and the package cover.

3.4 Bulk Waves

Besides the desired surface waves, interdigital transducers launch waves into the bulk of the material. These waves can be reflected from the base of the crystal and cause interference and noise at the output transducer. Exact analysis of bulk wave power and spectra

have been published[11]. These results indicate that several bulk modes exist which propagate with varied intensities depending on the crystal orientation. Choosing a crystal orientation which reduces a particular bulk mode at a given frequency does not necessarily allow for reduction of other bulk modes. The elimination of the bulk wave interference, thus, rests on the absorption and scattering of bulk modes at the base of the crystal or upon several other schemes[21] which increase the complexity of the design. One such design is to taper the crystal bottom so as to skew the bulk wave wavefront. The effect at the output transducer is to produce destructive interference in the bulk wave power received. Another similar scheme is to offset half of the output transducer to produce the same effect. None of these methods, however, reduce the power loss at the input transducer since the waves are still generated; however, there are other more significant losses to consider as discussed in section 1.6.

The velocity of waves in the bulk is greater than surface waves. For $LiNbO_3$, the bulk wave velocities in the Z propagation direction are $v_\ell \geq 7287$ m/s and $v_t \geq 3547$ m/s in comparison with the surface wave velocity of 3488 m/s (the subscripts ℓ and t stand for longitudinal and shear respectively). For this reason, bulk wave interference occurs at frequencies higher than the synchronous frequency. This is apparent since bulk and surface waves share the same periodic generating structure. The bulk wave travels downward at angle θ from the surface. Thus, its propagation constant is related to the SAW propagation constant by

$$k_b = k_s \sec\theta, \; k = 2\pi f/v \tag{3.4.1}$$

From this

$$f_b = (v_b/v_s) \; f_o \sec\theta \tag{3.4.2}$$

For the case of $LiNbO_3$, shear wave interference will occur at frequencies greater than 1.017 times the synchronous frequency. Longitudinal waves will occur at frequencies greater than 2.089 times the synchronous frequency. Milsom has shown[11] that for YZ-$LiNbO_3$ the maximum shear amplitude occurs at twice the synchronous frequency. A maximum also occurs in the longitudinal amplitude but the maximum is only about 20% of the shear. Experimentally, it has been found that roughening of the crystal base and use of an absorber such as Apiezon grease, reduces the bulk wave power to a negligible value. The bulk waves are noticeable, however, and result in a slightly decreased sideband suppression on the higher frequency side of any SAW filter response.

3.5 Group Delay in Presence of Distortion

When both reflections and electromagnetic feedthrough distort the filter response, the result is an asymmetric ripple dependent on the relative magnitudes and phase shifts of the signals.

The treatment of combined reflection and feedthrough is complex and will not be given here. Instead, a study of the group delay of the reflected wave distortion will be given which should provide an upper bound on the deviation from linearity.

The phase of the reflected wave amplitude is given by

$$\phi(f) = \tan^{-1}\{r^2\sin\theta/[1 - r^2\cos\theta]\} \qquad (3.5.1)$$

where

$$\theta = 4\pi f\ell/v_a + 2\phi_r \qquad (3.5.2)$$

The group delay using equation (1.7.1) is

$$T(f) = -r^2(2\ell/v_a)(\cos\theta - r^2)/(1 + r^4 - 2r^2\cos\theta) \qquad (3.5.3)$$

This group delay has minima at $\theta = (2n+1)\pi$ and maxima at $\theta = 2n\pi$, where $n = 0, \pm 1, \pm 2, \ldots$

Thus, the change in group delay due to phase ripple is given by

$$\begin{aligned}\Delta T &= [T(f)]_{max} - [T(f)]_{min} \\ &= 4\ell r^2/[v_a(1 - r^2)] \end{aligned} \qquad (3.5.4)$$

With regard to the INTELSAT specifications of Figure 1.1, assuming that the range of f is restricted to between 65.2 MHz and 74.8 MHz and also that the change in group delay due to other influences has magnitude less than 1 ns, the change in group delay must be less than 2 ns over the 9.6 MHz range.

Since ripple is periodic and it is assumed that the period is less than 9.6 MHz:

$$\Delta T < 2 \text{ ns} \qquad (3.5.5)$$

For $LiNbO_3$, the acoustic velocity, v_a is 3488 m/s. Assuming $\ell = 1$ cm, this gives $r \approx 0.0132$. Provided no loss external to the transducers is employed, this means the peak to peak ripple amplitude must be

$$\begin{aligned}R_{pp} &= 20 \log |(1 + r^2)/(1 - r^2)| \\ &\approx 0.003 \text{ dB}\end{aligned} \qquad (3.5.6)$$

This ripple is too small to be practically achieved without external loss mechanisms such as electrical mismatch or a 45° reflecting layer

situated between the transducers. Both these mechanisms increase the insertion loss of the device which may not be tolerable.

3.6 Alternative Methods of Ripple Suppression

For reflected waves, double electrode structures, as shown in Figure 3.5, are commonly used to reduce ripple. The wave reflections are such that destructive interference results and no reflected wave propogates. The disadvantage of this technique is the strain it places on the fabrication system, since twice the resolution is required, and the increased electrode resistance.

A novel idea which could potentially cure both reflected wave and electromagnetic feedthrough distortion also relies on the fidelity of the fabrication system. If curved transducers were skewed apart, as in Figure 3.6, perpendicular to the finger length, such that the distance between the independent strips was an integral number of wavelengths, the period of the ripple could theoretically go to infinity; that is to say, there would be no ripple since reflected waves would add in phase at all frequencies. This argument relies on the independence of elementary strips which conceptually form the composite transducer and on the assumption of no diffraction.

In practice, the ripple period would be determined by the error in the fabrication process. For instance, if the transducers could be aligned such that the error in separation is ϵ, the period of the ripple would be $v_a/(2\epsilon)$. Since a 100 times reduction is used for the experiments in this thesis, an error of $\pm$ 1/10" results in a ripple

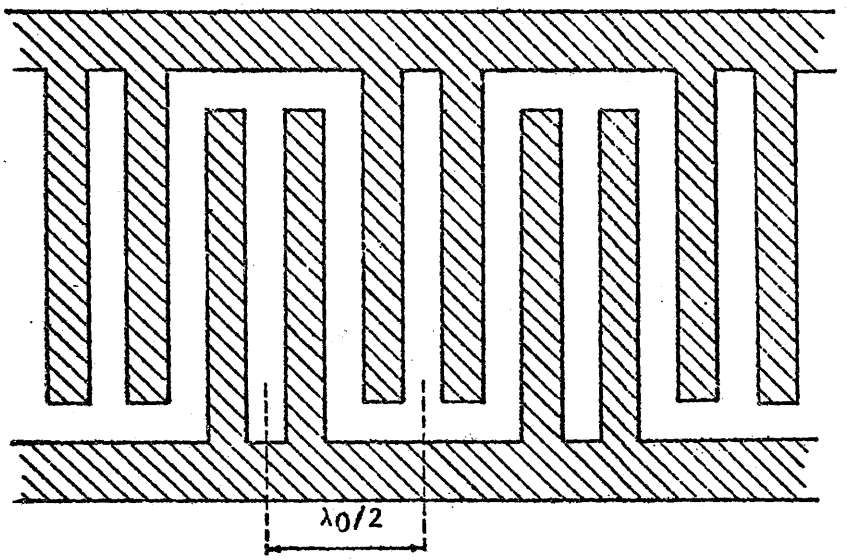

Figure 3.5 Double Electrode Structure for Elimination of Passband Ripple of Reflective Origin

Figure 3.6 Illustrating Skewed Transducer Design for Increasing the Period of Passband Ripple

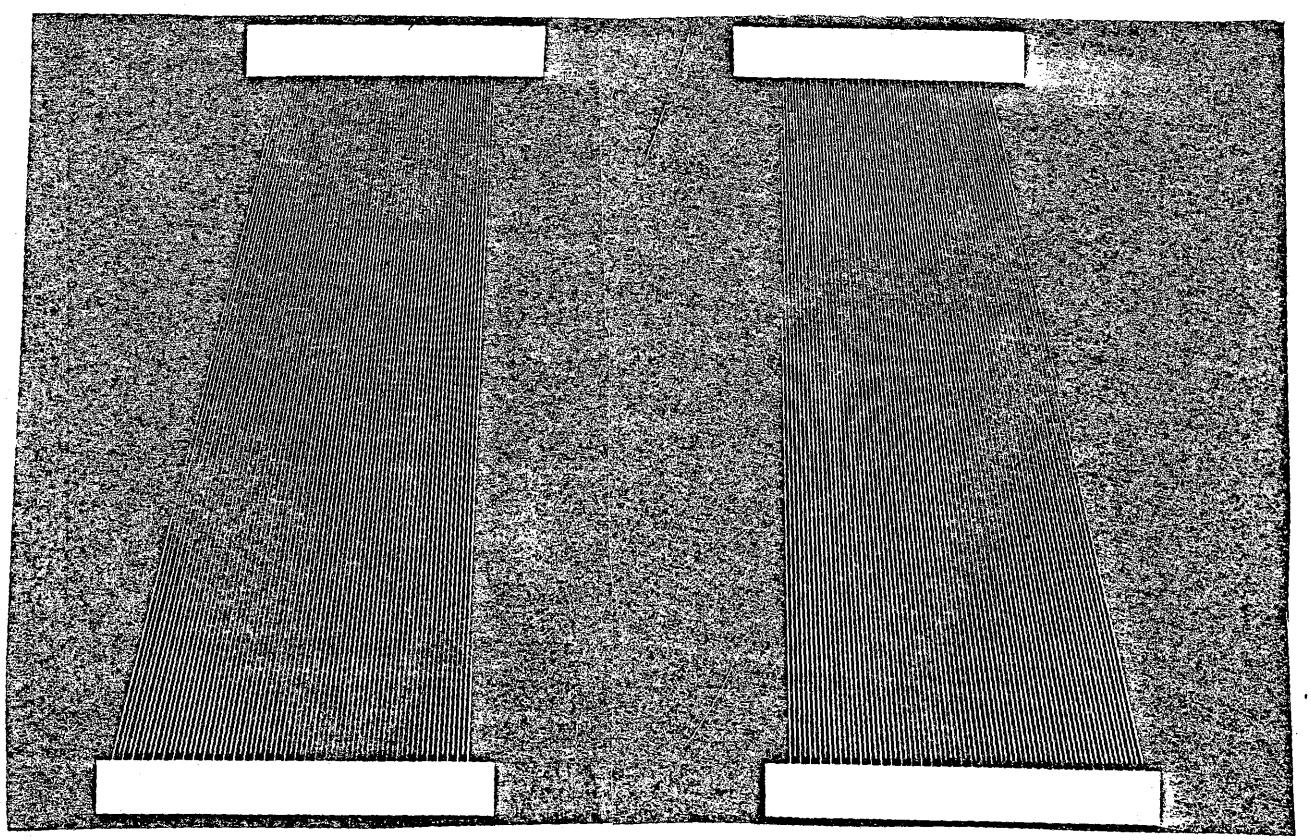

period of 70 MHz on $LiNbO_3$.

A substantial problem with this approach is the fact that care has to be taken to account for the phase shift which occurs on reflection and with electromagnetic feedthrough. It may be possible to set the transducer spacing to bring the reflective ripple and the feedthrough ripple into phase. A method for positioning the minimum (or maximum) of the resultant ripple at the centre frequency is discussed in the next section.

3.7 Phase Compensation

The use of a metallic strip deposited between the transducers can correct any adverse phase shift in the system within the limits of accuracy of the lithographic system[22]. Since the curved finger transducer effectively decouples frequencies along the aperture, an arbitrary phase shift with respect to frequency can be imposed by varying the width of the strip.

The effective phase shift due to velocity change under a metallized region is:

$$\Delta\phi = + \pi k^2 L/\lambda \qquad (3.7.1)$$

where L is the width of the strip. For $LiNbO_3$,

$$\Delta\phi = + .14\ L/\lambda \qquad (3.7.2)$$

For good reproduction and to minimize the effect of etchant undercutting in the fabrication process, a finite phase shift should be imposed at all frequencies.

CHAPTER 4

FABRICATION OF SAW FILTERS

4.1 General

Fabrication of SAW filter devices involves two distinct stages. The first is the construction of conducting strips or electrodes on a piezoelectric substrate according to the filter design specifications. The second stage is the packaging of this active component to allow hookup with conventional systems, and to maintain the device characteristics. These stages are discussed here; in subsequent sections, the procedures developed and used for the experimental work in this thesis are treated.

4.1.1 Construction

The electrode separation desired in SAW filter design is of the order of 50 μm. The aperture is typically 0.5 cm. Thus, there is a need to satisfy the demands of high resolution over a relatively large area. Since photographic techniques far exceed any comparable mechanical system in terms of resolution and repeatability, advantage is taken of the photolithographic process. There are six main steps in the process:

1. A piezoelectric crystal is coated with aluminum and then a material called photoresist.
2. A photomask of the desired electrode structure is prepared.

3. The photoresist is preferentially exposed using this photomask.
4. The activated photoresist is dissolved in a specially prepared solvent.
5. The aluminum not covered by the remaining photoresist is etched away, leaving the desired pattern.
6. The remaining photoresist is removed with acetone.

4.1.2 Packaging

The proper packaging of the active component is essential to the initial and long term success of the device. Care must be taken not to degrade the crystal or its electrode structure in any way, and to provide containment free from contamination. (Sometimes heaters are included in SAW packages to reduce the effect of temperature.[20]) The introduction of unaccounted for distributed reactance or resistance must be avoided or, at least, minimized.

There are four basic steps in the packaging process:

1. Construction of a grounded container complete with connectors compatible with the intended application.
2. Insertion of the crystal on a bed of absorptive material to reduce bulk wave and end reflection interference.
3. Positive mechanical attachment of the crystal to the container.
4. Hookup of transducers to the connectors.

4.2 Preparation of Crystals

In this writing, the topics of orientation, cutting and polishing of the crystal substrates, although important in themselves, will not be covered. For the most part these operations are handled by the retailers of such materials and this application does not constitute a significant departure from established technique. For further information on these subjects, however, the reader is referred to Smith[17].

The cleaning of the crystals prior to use is a widely varying procedure and, for this reason, the process is described here. The proper cleaning of the crystal cannot be over-emphasized especially considering the microscopic dimensions of the active regions of the final device.

Cleaning begins by removing any obvious contaminants such as residual black wax, Apiezon grease, RTV silicone rubber, silver paint, photoresist, and aluminum from past devices.

Soaking in trichloroethylene dissolves most organic substances effectively including black wax and Apiezon grease. RTV is removed by application of (weak) acetic acid. Similarly, silver paint and photoresist are dissolved by acetone. At this point any aluminum deposits on the crystal can be removed by an appropriate aluminum etch. (The etchant used in this application consists of 25 parts H_3PO_4, 5 parts CH_3COOH, and 1 part HNO_3.)

Each crystal is then mounted on a Headway Spinner Unit, held by vacuum, and subjected to a more vigorous scrubbing with a cotton swab

soaked in turn with trichloroethylene, acetone and distilled water. After spinning dry, a fresh cotton swab is selected and the scrubbing continues with trichloroethylene, acetone and then methanol. After a final spin dry, the crystals are transferred to a clean, covered Petri dish, using tweezers or handling them only by the edges.

When ready to evaporate a thin film of some material onto the crystals, they are removed from the Petri dish and placed polished side facing the evaporant in the vacuum chamber but separated by a shutter. The system used is an Edwards Model 12E3/1670 High Vacuum Coating Unit, shown in Figure 4.1. Once the chamber has been evacuated the final stage of cleaning is performed. At a pressure of 10^{-1} torr, the high vacuum valve is closed and argon gas is allowed to enter the chamber. Through the use of a high voltage element within the chamber, enough energy is imparted to the argon atoms that they microscopically clean the crystals by collision once the shutter has been opened. This continues for approximately twenty minutes, at which time, the high voltage element is switched off, the shutter closed, the chamber allowed to cool, and the argon gas evacuated. Evaporation commences once the chamber has been pumped down to reasonably low pressure ($\approx 10^{-5}$ torr).

First, the voltage for the filament containing the material to be evaporated is switched on with the current turned off. Slowly the current is increased to avoid rapid melting of the material which could result in loss of material and possible shorting of the filament. Once the current reaches approximately 20 amps, impurities in the material begin to evaporate. The shutter should be opened only after sufficient

Figure 4.1 Photograph of Vacuum System and Mask Aligner

time has elapsed for the impurities to be pumped out.

When ready, the current is increased to about 30 amps, the shutter opened and the thickness of material deposited may be recorded from the decrease in natural oscillation frequency of the in-chamber quartz oscillator which is measured and displayed by supporting electronics. The frequency is related linearly to the thickness of material deposited for small thicknesses and frequency deviation less than 200 KHz from the original resonant frequency of f_o = 6 MHz by the following formula:[8]

$$t = - 10\ \Delta f\ \rho_q\ t_q/(f_o\ \rho_m) \qquad (4.2.1)$$

where

t = thickness (Å)

Δf = change in resonant frequency (MHz)

ρ_q = 2.651 g/cm^3 (density of quartz)

t_q = 0.6 mm (thickness of quartz crystal)

ρ_m = density of material deposited (g/cm^3)

For aluminum, ρ_m = 2.699 g/cm^3, and the thickness is approximately equal in value to the frequency change.

After the desired thickness is reached, the shutter is closed and the remaining material evaporated from the filament. The filament is then switched off and the chamber allowed to cool before breaking vacuum.

When the crystals are removed from the vacuum chamber, they may be coated with a thin layer of Shipley AZ1350B positive photoresist. Each crystal is mounted on the spinner and a pipette is used to deliver

several drops of filtered photoresist onto the crystal. The crystal is spun at 4000 rpm for approximately 30 seconds to achieve a fairly uniform thickness. The linewidth accuracy depends on the uniformity of the photoresist layer, as the photomask is brought into intimate contact with the coated crystal. However other factors such as photoplate and substrate flatness and the presence of dust usually are the accuracy determining factors.

4.3 Preparation of Photomask

To obtain the resolution necessary for SAW filter masks, it was necessary to cut and subsequently photoreduce a large scale prototype mask. To realize a consistent resolution, to assure complete flexibility and repeatability, and due to the complexity of the desired patterns, the oversize masks were cut under computer control. An added advantage of this approach was the time savings involved. Masks could be cut in less than an hour with the completed system which would take days by hand.

For computer generation of masks to take place, the mask must be given as a sequence of elementary cutting operations. These elementary operations are defined as movements of the knife from an initial to a final position with the knife either held inactive (up) or cutting (down). Due to the periodic nature of the masks considered, certain macro-operations can be defined which perform the cutting of an individual electrode. The final cutting sequence is not unique and can be optimized in terms of number of cutting operations.

4.3.1 Cutting Prototype Mask

Two computer systems were used in the preparation of masks. The McMaster University CYBER 170 mainframe was used for the bulk of the computational effort needed to digitise and transform a desired structure into a cutting sequence. An INTEL SDK-8085 microprocessor-based computer system was used for the actual cutting of the masks.

By using the CYBER to convert the cutting sequence data into a form which the microprocessor could interpret, the data could be read in through an Omnitec modem/telephone link and stored by the microprocessor on a Triple I Phi-deck cassette tape peripheral. This equipment is shown in Figure 4.2. This step essentially releases the CYBER from further on-line operation, eliminating excessive costs for computer time, and providing a self-sufficient facility freed from the burden and delays of time-sharing.

The cutting of Ulano Rubylith, a sheet of tough, transparent mylar laminated with a soft, optically dense polymer, is done on a Haag-Streit 120 cm x 120 cm coordinatograph (cutting table) shown in Figure 4.3. Superior Electric Slo-Syn Stepping Motors (200 steps/rev) with a 5:1 gear reduction were added to yield a resolution of .001". Superior supplied a translator module which provided the motor control in response to external digital input. The microprocessor could be interfaced to this module and control the motors in accordance with the stored data.

The specific operation of the microprocessor system is not covered in this thesis but may be found in Zeuner.[23] Similarly,

Figure 4.2 Photograph of SDK-8085 Microprocessor System and Supporting peripherals (l. to r.): Omnitec Modem, Lear Siegler ADM-3A CRT; (top shelf) SDK-8085 and Communications Interface board, Triple I Phi-deck cassette deck; (bottom shelf) Lambda power supply, Motor Interface board, Marsland Teletype.

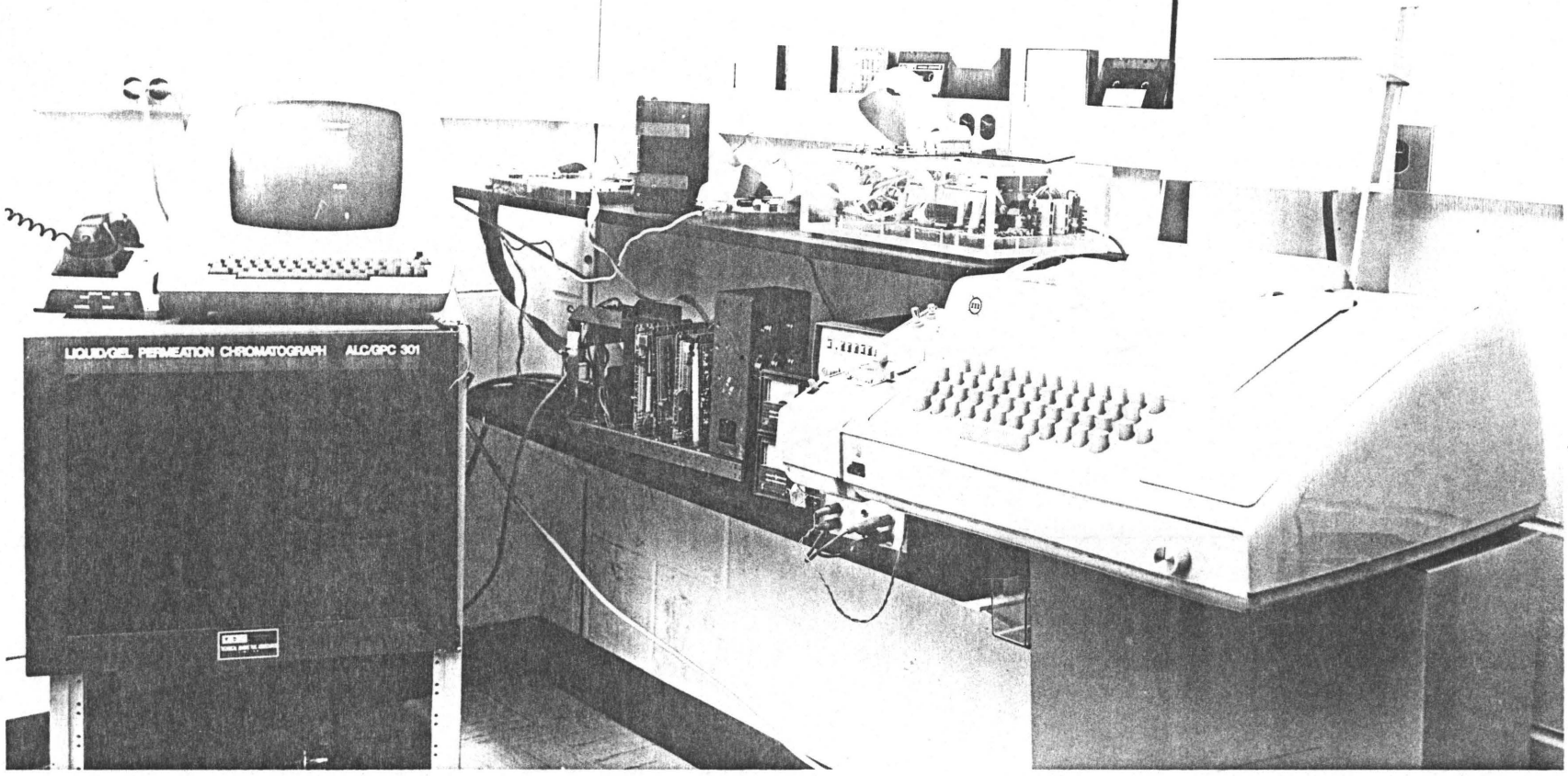

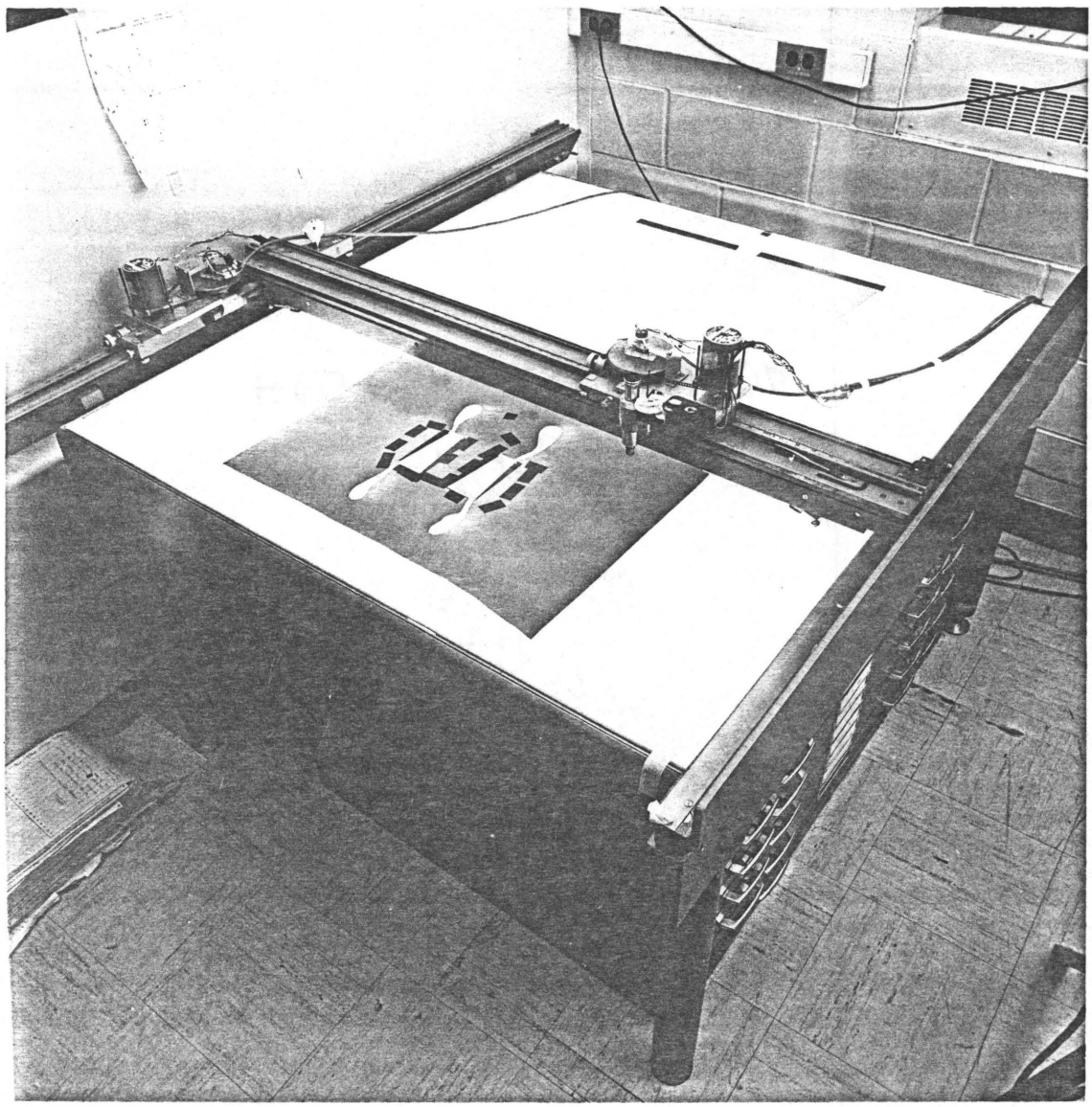

Figure 4.3 Photograph of Cutting Table and Stepping Motors. Note oversize prototype mask (background) and photoreduced mask (foreground).

assembly language software written by the author will not be documented here; the reader is again referred to Zeuner. Copies of the FORTRAN programs written for this thesis, however, are given in the appendix.

When the microprocessor finished the cutting task, the mask was completed by defining the connections between the two sets of fingers which become the bus bars in the final device. Unwanted rubylith was then peeled away from the mylar underlay leaving a positive photomask. A peeled mask is also shown in Figure 4.3 along with its photoreduced counterpart.

4.3.2 Preparation of the Cutting Table

The surface of the cutting table was cleaned with alcohol prior to any cutting job to avoid unecessary knife wear and to give good rubylith adherence to the cutting surface which resulted in an undistorted mask.

The rubylith was then cut to size and fastened securely, dull side up, to the surface with masking tape. Care was taken not to overly stretch the rubylith which could have also resulted in a distorted mask once the tape was removed.

The knife was then inserted in the holder and the entire assembly manually positioned to the desired starting position.

4.3.3 Cutting Knife

The choice of a cutting knife must be based on the following characteristics:

1. Directionality: The knife must cut uniformly in all directions. Since a mechanism for rotating the knife is not available at this time, a spherical tip is essential.
2. Weight: Tearing of the rubylith occurs when a knife which is either too dull or too heavy is used.
3. Durability: The knife should be able to cut at least a complete mask without compromising the resolution by excessive wear.
4. Compatibility: The knife designed should fit in the holder attached to the movable assembly.

Knives supplied by manufacturers were not designed for omnidirectional operation, so a substitute had to be found. To immediately satisfy requirements 2 and 4, however, the models tested were modifications of these supplied knives.

The first model was made simply by turning down the end of one of the steel knives supplied on the lathe at an angle of approximately 20^{o}. This was found to give an acceptable cut but was subject to excessive wear. Periodic sharpening with fine grain sandpaper under the microscope resolved this problem temporarily but gradually the tip became so dull that it needed to be turned down again. Naturally this process leads to a lighter knife which necessitates complete replacement. A more durable model was found in setting a seamstress' pin in a small hole drilled in the end of the steel rod. Fast drying epoxy was found to fix the pin fairly firmly in the hole.

The finer tip of the pin allowed for a greater wear before resharpening or replacement was necessary. The possibility that a fine

needle might provide an even more durable tip is being investigated.

4.3.4 Photoreduction

A custom-built camera system equipped with a Schneider "Repro-Claron" lens provided a 5X reduction of the photomask. The system has a maximum object size of 22.5 x 22.5" and a resolution of 10-20 lines/mm. Due to the limited object size each transducer was reduced separately and subsequently realigned prior to the second photoreduction. It was found that with existing illumination an exposure of 2 minutes with the aperture set to approximately 3 mm diameter, followed by 1 1/2 minute development at room temperature gave an acceptable compromise between high contrast and good resolution. Kodak 5" x 7" Graphic Arts Film (CAT 163 8808) was used.

The transducer patterns were cut out of the resulting negatives and mounted onto a window cut in a fresh sheet of rubylith. At this time the proper orientation and separation of input and output transducers was ensured. Transducer pads were also cut out which later were used for connection of the transducers to external terminals.

The second stage of photoreduction was performed using a Microkon 1700 camera with a resolution of 200 lines/mm. This stage produced a further 20 x reduction resulting in an overall 100X reduction. With an aperture of 13 mm and available illumination it was found that a 10 sec exposure and 1 1/2 minute development gave good results. Kodak 2" x 2" x .06" High Resolution Plates (CAT 173 2791) and a 4:1 dilution of room temperature Kodak HRP developer were used.

Both the 5" x 7" film and the HRP's were fixed for approximately 3 minutes using liberal amounts of prepared, room temperature, Kodak fixer (CAT 123 8146) before rinsing in de-ionized water and being blown dry with compressed dry nitrogen. Such fixing is essential for the plates as they come in direct contact with the crystal surface. If they are not fixed, the emulsion is not hardened and may be smeared by relative motion between the crystal and the plate.

4.4 Photoresist Exposure and Etching

The photomask pattern was transferred to the photoresist coating of the crystal using a Kasper Model 7001 Mask Aligner shown in Figure 4.1. This system allows the user to position the crystal relative to the photomask under magnification to avoid localized surface contamination and to achieve accurate alignment of the transducer pattern along the propagation axis of the crystal defined by the crystal cut. The mask and crystal were brought into intimate contact after alignment and exposed to ultraviolet light. Eight seconds exposure was found to be sufficient for prevailing light conditions. It was important to remember to keep the emulsion side of the plate facing the crystal to avoid light diffraction through the thickness of the plate. The photoresist was then developed using 40 ml of full strength Shipley AZ developer at room temperature. The photoresist which was not shielded from ultraviolet light by the photomask was dissolved by the developer revealing the aluminum beneath. The development time is not very critical since unactivated photoresist is not very soluble. The

pattern was visible when observed at an oblique angle in a matter of seconds.

The crystal was then rinsed in deionized water and submerged in a Petri dish containing the aluminum etch described in section 4.1. The etching time is not extremely critical but the process should be observed carefully, if possible, under a microscope, to prevent undercutting and ensure good metallization ratio. The actual time depends on the agitation of the crystal in the etchant but is of the order of half a minute at room temperature.

The etched crystal is rinsed in deionized water and then flushed with acetone which dissolves the remaining photoresist. After blowdrying with compressed dry nitrogen the crystal is ready for packaging.

4.5 Packaging

The packages used for the experimental SAW filters were aluminum boxes fitted with SMA connectors. In preparation for crystal packaging, the boxes were cleaned to remove any macroscopic contamination such as RTV, black wax, grease and silver paint. The floors of the boxes were scraped to ensure good electrical contact.

The crystal was placed in the package on a bed of Apiezon grease, taking care that the grease does not extend beyond the crystal boundaries. The grease acts as an absorber of bulk waves, but must not be allowed to short out the device or otherwise interfere with its operation.

RTV was then applied to both ends of the crystal to both fasten the crystal down securely upon drying and to prevent end reflections of surface waves. RTV will flow somewhat before drying but it should not be allowed to cover any part of a transducer.

When the RTV was sufficiently dry, GC silver paint was used to connect .001" diameter gold wire (provided by Sigmund Cohn corp.) between the transducer pads and the input and output connectors. The floor of the aluminum box is commonly used as a ground terminal in devices not using balanced transformers. The silver paint must be left to dry overnight before it becomes fully conducting. The electrical characteristics of the gold wires are summarized below using formulae adapted from Kraus and Carver.[7]

$$R' = \rho/(\pi r^2) \simeq .464\ \Omega/\text{cm}$$

$$L' \simeq (\mu/2\pi)\ \ln|2h/r| \simeq 13.3\ \text{nH/cm} \qquad (4.5.1)$$

$$C' \simeq 2\pi\varepsilon_o\varepsilon_r/(\ln|2h/r|) \simeq .0834\ \text{pf/cm}$$

$\rho \simeq 2.35\ \mu\Omega\text{-cm}$ $\qquad$ $\varepsilon_r \simeq 1$

$r \simeq 1.27 \times 10^{-3}$ cm $\qquad$ $\varepsilon_o = .0885$ pf/cm

$h \simeq .5$ cm $\qquad$ $\mu = 4\pi$ nH/cm

here, h represents the distance between the goldwire and the ground plane. These formulae are very approximate and serve only as a rough guide to the effect of the gold wire. Obviously the distance between the terminal and the transducer bus bar should be minimized. Other capacitive effects may be due to the amount of silver paint used. For a spot size of r = 1 mm (radius) and crystal thickness t = 0.05 cm

$$C = \varepsilon_o \varepsilon_r \pi r^2/t$$

$$\simeq 1.6 \text{ pf}, \varepsilon_r = 29 \ (LiNbO_3)$$

$$\simeq .25 \text{ pf}, \varepsilon_r = 4.6 \text{ (quartz)} \qquad (4.5.2)$$

Finished packages are shown in Figures 5.3, 5.6 and 5.9.

CHAPTER 5

RESULTS AND CONCLUSIONS

5.1 Experimental Considerations

This chapter presents the results and conclusions of experimental trials in which actual SAW filters were designed and constructed. Ten successful devices were made which represent four different mask patterns.

All devices were constructed on a YZ-lithium niobate ($LiNbO_3$) substrate. The pertinent parameters for this substrate are summarized in Table 5.1 relative to other common piezoelectric materials. It may be noted that $LiNbO_3$ also has the features of autocollimation discussed in Section 3.1.

Crystals, precut and polished by the supplier, had a roughened base to enhance scattering of bulk waves, as well as an application of bulk wave-absorbing grease as discussed in Section 4.5. the thickness of evaporated aluminum was roughly 500 Å for each device with a metallization ratio of $\eta \approx 1/2$.

Three different finger curvatures were used, the curve being given as

$$x = W\,(f_o^{\,p} - f_1^{\,p})/(f_h^{\,p} - f_1^{\,p}) \qquad (5.1.1)$$

were p takes the values 1, -1/2, and -1. The latter value corresponds to slanted finger transducers.

5.2 Test Equipment

All devices made were tested on the HP 8085A Network Analyzer shown in Figure 5.1. This instrument permits measurement of the transfer function amplitude and phase characteristics of the device under test. The frequency range of the analyzer is 500 kHz to 1300 MHbz with a dynamic range of 100 dB. Up to five markers can be used to accurately measure the response at continuously variable frequency locations.

The HP 8501A Storage-Normalizer, also seen in Figure 5.1, allows labels to be displayed on the screen as well as providing trace storage and trace averaging capabilities.

Details of the operation of these instruments can be found in the reference manuals supplied with the instruments. For the purpose of testing the experimental devices, the following settings were used:

Frequency range: 500 kHz to 130 MHz

Scan time (continuously variable): .1 to 1 sec.

Electrical length: to compensate for lead length, producing zero phase shift on calibration.

Filters: 10 kHz bandwidth

S-parameter measured: S_{21} (forward transfer characteristic)

No video filter or averaging was used.

5.3 Data Presentation

The experimental design parameters for five selected devices are given in Table 5.2 followed by the experimental response parameters in

Table 5.3. These devices test the effects of transducer separation and acoustic aperture on distortion. Also, the relation between finger curvature and passband slope is demonstrated. Most of the devices conform to identical, 71 finger (35 finger pairs) input and output transducers operating at a centre frequency of 70 MHz, and a 50% band width. An enlarged view of the mask pattern, a photograph of the finished device, and the filter response are given for the last three devices in Figures 5.2 to 5.10, inclusively. For device 5, two closer views of the response follow in Figure 5.11 and a photograph of the group delay response and Smith Chart analysis are shown in Figure 5.12. The last figure shows a comparison between the response of device 2 and a sixth device. These results are studied in the next sections with regard to overall characteristics, distortion, transition bandwidth, group delay and passband slope.

A brief explanation of the filter response photographs taken directly from the Network Analyzer CRT display is in order. Referring to Figure 5.4, the upper photograph presents the amplitude and phase characteristics of the slanted finger transducer. Two horizontal lines mark the reference position at time of calibration for each trace. The vertical scale is clearly displayed in the upper left and right hand corner while the horizontal scale is given in terms of START and STOP frequencies which refer to the left and rightmost graticule, respectively. The magnitude and phase response at the marker located here at the centre of the trace is displayed also in the upper left and right hand corner. The frequency corresponding to the marker position

is given at bottom centre. The insertion loss at the marker position is given by the sum of the marker amplitude in the figure and the reference offset given in the caption. Thus for this response the insertion loss is IL = -(15.6 dB - 52 dB) = 26.4 dB. The reference phase offset is given in the caption as well, but absolute phase measurements are not of interest at this time. The lower photograph shows the response of the same device with an enlarged frequency scale. For some photographs, like this one, the frequency scale is given as a continuous wave (CW) reference located at the centre of the screen and a sideband ΔF. Thus this lower figure has a frequency range of 67 MHz to 73 MHz or 0.5 MHz/div.

5.4 Overall Characteristics

In terms of centre frequency, bandwidth, and group delay the experimental test results conform well with design specifications of Table 5.2 and the theoretical predictions of Chapters 2 and 3. The phase response seen in Figures 5.4, 5.7 and 5.10 shows the nominally linear phase expected with symmetrical SAW filters. (The phase response is displayed modulo 360° meaning that after each 360° excursion the sweep returns to 180° above the reference line. This trace can be used for measurement of the SAW velocity since each period corresponds to the filter delay time and since the transducer separation is known). Furthermore, the transition bandwidth is adequate in most cases with respect to the constraints of Figure 1.1. However, large variations and discrepancies were found in the measurement of insertion loss, passband

ripple amplitude, passband slope, and sideband suppresion. The reasons for the differences can be attributed to nonconformity of the fabrication process, particularly in the control of metallization ratio and packaging techniques.

The metallization ratio, as explained in Section 4.4, depends on the etching time. Since each crystal was processed individually a variation in metallization ratio is to be expected. It is also possible that undercutting of the metal electrodes was occurring unobserved. This can produce three effects. First, an increase in electrode resistance due to narrower fingers constitutes a greater loss in the system. Secondly, from Figure 1.4, a change in metallization ratio from .4 to .6 can result in a 2.6 dB change in acoustic wave generation by the IDT. Thirdly, finger pair capacitance, C_s, is influenced by metallization ratio as described by Naraine[13]. Obviously, there is a need for a more consistent and accurate etching procedure in the production of SAW devices.

Packaging consistency is a major problem at the present time since the application of silver paint in the hookup of the device can create large stray capacitance through the thickness of the crystal. The spatial relationships in a package also greatly affect the field characteristics and, therefore, the electromagnetic feedthrough. Experimentally, three different package sizes were used, two of which are shown in Figures 5.6 and 5.9. The 90° positioning of SMA connectors as shown in Figure 5.3 seems to have improved the ripple characteristic of device 3 since, for the same transducer separation in a device with

facing SMA connectors, the ripple would exceed 7dB.

Device 3, however, suffers from increased bulk wave interference by comparison of Figure 5.4 with Figure 5.7. This results from the absence of an absorbing grease layer under the crystal. As predicted in Section 3.3, the bulkwave power is confined to frequencies higher than the lowest frequency in the passband. The loss in sideband suppression due to this effect is also evident.

Another factor involved in packaging is the length of connecting wire used. The gold wires used act as a transmission line ($Z_c \simeq 400\ \Omega$) which result in electromagnetic reflection towards the generator. The presence of the short transmission line transforms the apparent source impedance, as seen by the transducer, to one with both resistive and inductive components. Finally, it is noted that the characteristics of the devices changed considerably in terms of insertion loss over a period of one month. This may be due to contamination or oxidation of the aluminum electrodes, thus, some protective agent, perhaps a hermetic seal is in order.

The anticipated use of an ultrasonic gold wire bonder in the near future should solve many of these problems with the adoption of standard packaging procedures. The shorter lead lengths and the absence of silver paint will greatly reduce the insertion loss and improve the repeatability of experiments. In addition, some means of electrically isolating the transducer from ground should be employed to reduce capacitance, perhaps by inserting a thick insulating layer of low dielectric constant between the crystal and the ground plate.

Naturally, all the effects described here could be incorporated into the equivalent circuit model of Section 1.6, for each device; however, the error in the estimation of the geometrically dependent factors such as electromagnetic feedthrough would not produce a particularly reliable result. The effect of stray capacitance can be easily demonstrated by the inclusion of an extra capacitive term in equation (1.6.11). This has been done and the results summarized in Table 5.4. It is shown that the presence of stray capacitance results in increased insertion loss and decreased high frequency end response, as expected. The slopes and insertion loss values calculated actually concur in several cases with experimental results even though the calculation to extremely crude.

5.5 Distortion Study

With the considerations of the last section in mind, a few general statements regarding the nature of passband distortion can be made. In the filters constructed, it was found that electromagnetic feedthrough was the greatest contributor to ripple distortion. This can be seen by referring to the lower figures in each of the three filter responses presented. The correlation between ripple period and transducer separation is very good, assuming dominant electromagnetic feedthrough, as a comparison of column ℓ in Table 5.2 and ℓ' in Table 5.3 will show. With devices 4 and 5, the ripple amplitude is reduced from 6.6 dB peak-to-peak to less than 1 dB peak-to-peak. This compares well with the expected change in ripple due to transducer separation.

5.6 Transition Bandwidth and Sideband Suppression

Transition bandwidth is influenced by the number of fingers in the filter. A sharp transition band requires a large finger number. Sideband suppression is determined by the presence of bulk waves which can be seen in Figures 5.4a) and 5.7a) on the high frequency end. Sideband suppression is within the desired value of 25 dB for the filters not subject to excessive ripple distortion which lowers the passband amplitude.

These two parameters do not impose great constraints on the design and are quite easily satisfied.

5.7 Group Delay

Here, the validity of equation (3.5.4), developed in pursuit of group delay deviation due to ripple distortion, is demonstrated. The ripple evident on the passband of device 5 shown in Figure 5.10b) is chiefly due to internal wave reflections, judging from the ripple period. The maximum peak-to-peak ripple is easily measured to be $\simeq$ .91 dB, as given in Table 5.3, which corresponds to a reflectivity of $r^2 = 0.053$. From equation (3.5.6) and (3.5.4) it is seen that this reflectivity would result in a range of group delay of 0.43 μs. This checks quite well with the observed delay characteristics shown in Figure 5.12a), which confirms both the applicability of equation (3.5.4) and the assumption that circuit effects cause negligible group delay ($<$ 1.14 ns) as discussed in Section 2.4.3.

The methods for ripple suppression introduced in Section 3.6

involving skewed transducers appears to offer the most promising solution to the problem of assuring linear phase (constant group delay). Experiments need to be conducted which will determine the ability of the phase compensators of Section 3.7 to position the minimum of the ripple period at the centre frequency.

5.8 Passband Effects

Aside from distortion, the important passband effects are inherent passband ripple and passband slope. The effect of identical transducers on inherent ripple is manifested in the small but noticeable ripple which forms the envelope of ripple distortion due to acoustic reflections in Figure 5.10b) as well as the presence of horns or Gibb's phenomenon seen in Figure 5.11a) at the band limits.

Circuit effects are responsible for the average slope of the passband in Figure 5.11b) and those of Figure 5.13a) and b). Figure 5.13 shows clearly the ability to tailor the slope of the passband by altering finger curvature. The asymmetry evident in the upper trace is probably due to radiation susceptance which becomes large and positive (a negative inductance) for $f < f_c$ and smaller and negative for $f > f_c$.

5.9 Conclusions

Basic SAW theory was introduced in Chapter 1 which outlined the mechanisms and limitations of conventional work. The proposed course of design research was given in Chapters 2 and 3. The fabrication of SAW filters was described in Chapter 4, while this chapter demonstrated some

of the effects mentioned in the preceding chapters.

Essentially, the problem of achieving very wideband filters was divides into two areas:

1 The use of curved finger transducer to realize an arbitrary passband response

2 The minimization of aberrations by proper transducer separation, orientation and packaging.

The final design involves the use of an advanced circuit model to account for spurious effects and choice of an appropriate finger curve to give the flattest response. Attention must be given to the radiation susceptance term which becomes important near the band edges. The group delay characteristic could be satisfied by skewing the input and output transducers, automatically satisfying the magnitude ripple specifications. The thrust of future work should be the implementation of the theory presented here, with preliminary investigations into such areas as reflection amplitude and phase from an array of electrodes, improved fabrication techniques and the effect of radiation susceptance.

Work not covered here, or, at least, only lightly touched on, which may require further experimentation includes:

1. A study of beam steering in curved finger transducers on an autocollimating substrate. The optimal orientation for maximum acoustic wave coupling between transducers may be deduced from this, as well as limitations on finger curvature to reduce diffraction losses.

2. The effect of velocity change under fingers. The acoustic wavelength is shorter by ≈ 2.6% under a metallized region (in $LiNbO_3$). This should be accounted for through the use of a reduced metal finger width, yielding an effective metallization ratio of 1/2.
3. The use of double electrodes structures. If the cost in terms of fabrication resolution is not too high, double electrode structures may provide a viable alternative to skewing of input and output transducers to reduce ripple. The presence of double electrodes, however, will not reduce electromagnetic feedthrough.

TABLE 5.1

PROPERTIES OF PIEZOELECTRIC SUBSTRATES FOR SURFACE WAVES

Material	Cut	Propagation Direction	Coupling Coefficient k^2(%)	Capacitance/Pair C_s (pF/cm)	v_a ($\times 10^{-5}$ cm/sec)	Temperature Coefficient of Delay (ppm/$^\circ$C)
Quartz	Y	X	0.23	0.55	3.159	-24
Quartz(HC)	-20° rotated Y	X	0.25	0.55	3.209	-32
Quartz(ST)	$+42.75^\circ$ rotated Y	X	0.16	0.55	3.157	0
$LiNbO_3$	Y	Z	4.5	4.6	3.488	+90
$LiTaO_3$	Y	Z	0.74	5.7	3.230	+35
$Bi_{12}GeO_{20}$	110	001	0.85	—	1.62	+130

From Ref. 21

TABLE 5.2

TRANSDUCER DESIGN PARAMETERS

Device No.	f_c(MHz)	Δf(MHz)	p	N_i	N_o	W(cm)	ℓ(cm)
1	77.3	35.0	1	71	23	.32	.22
2	77.3	35.0	1	71	71	.32	.65
3	70.0	35.0	-1	71	71	.45	.31
4	70.0	35.0	-1/2	81	71	.50	.56
5	70.0	35.0	-1/2	71	71	.25	.67

Legend: f_c - centre frequency; N_i, N_o - number of fingers in input/output transducer

Δf - bandwidth; W - acoustic aperture

p - curve parameter (see section 5.1); ℓ - centre-to-centre transducer separation

TABLE 5.3

TRANSDUCER RESPONSE PARAMETERS

Device No.	Passband Slope	IL (dB)	SS (dB)	$R_{pp}(\rho)$ min (dB)	$R_{pp}(\rho)$ max	T (MHz)	ℓ' (cm)
1	+	-	-	-	9.20(.485)	1.57	.222
2	+	30.0	25		<.6 (.035)	——	——
3	-	36.4	11	1.98(.113)	4.43(.250)	1.11	.313
4	+	43.8	13	2.09(.120)	6.96(.381)	0.63	.551
5	-	30.4	25	0.18(.010)	0.91(.052)	0.52	.668

Legend: IL - insertion loss (at centre frequency)

SS - sideband suppression

R_{pp} - peak-to-peak ripple amplitude

ρ - reflectivity corresponding to $R_{pp} = 20 \log|(1+\rho)/(1-\rho)|$

T - ripple period

ℓ' - transducer separation estimate from T.

TABLE 5.4

TRANSDUCER RESPONSE ANALYSIS

Device No.		G_a ($\times 10^3$)	B_a** ($\times 10^3$)	ωC_T ($\times 10^2$)	IL (dB)	ΔIL (dB)	IL' (dB)	ΔIL' (dB)
1	@ 67.3MHz	2.453(0.771)*	1.887(0.593)	2.179(0.685)	22.34	3.16	29.34	1.38
	@ 87.3MHz	4.128(1.297)*	-0.714(-0.224)	2.816(0.888)	19.18		27.96	
2	@ 67.3MHz	2.453	1.887	2.179	20.71	2.52	27.45	1.29
	@ 87.3MHz	4.128	-0.714	2.826	18.19		26.16	
3	@ 60 MHz	3.499	1.447	2.731	19.87	2.20	26.08	-3.39
	@ 80 MHz	3.499	-1.447	3.642	22.07		29.47	
4	@ 60 MHz	4.215(3.688)*	2.121(1.856)	3.468(3.035)	20.96	-1.24	26.72	-2.19
	@ 80 MHz	4.867(4.259)*	-1.662(-1.454)	4.624(4.046)	22.20		28.91	
5	@ 60 MHz	1.844	0.9278	1.517	19.29	-0.90	27.24	-2.05
	@ 80 MHz	2.129	-0.7270	2.023	20.19		29.29	

Legend: G_a : transducer radiation conductance ωC_T : transducer static susceptance

B_a : transducer radiation susceptance IL : insertion loss

ΔIL : average slope of response curve between frequencies listed

IL' : insertion loss with stray capacitance (50 pf) included

ΔIL' : average slope of response curve between frequencies listed with stray capacitance (50 pf) included.

Note 1* : Parentheses denote output transducer value if different from input transducer values.

Note 2** : Calculated through Hilbert transform

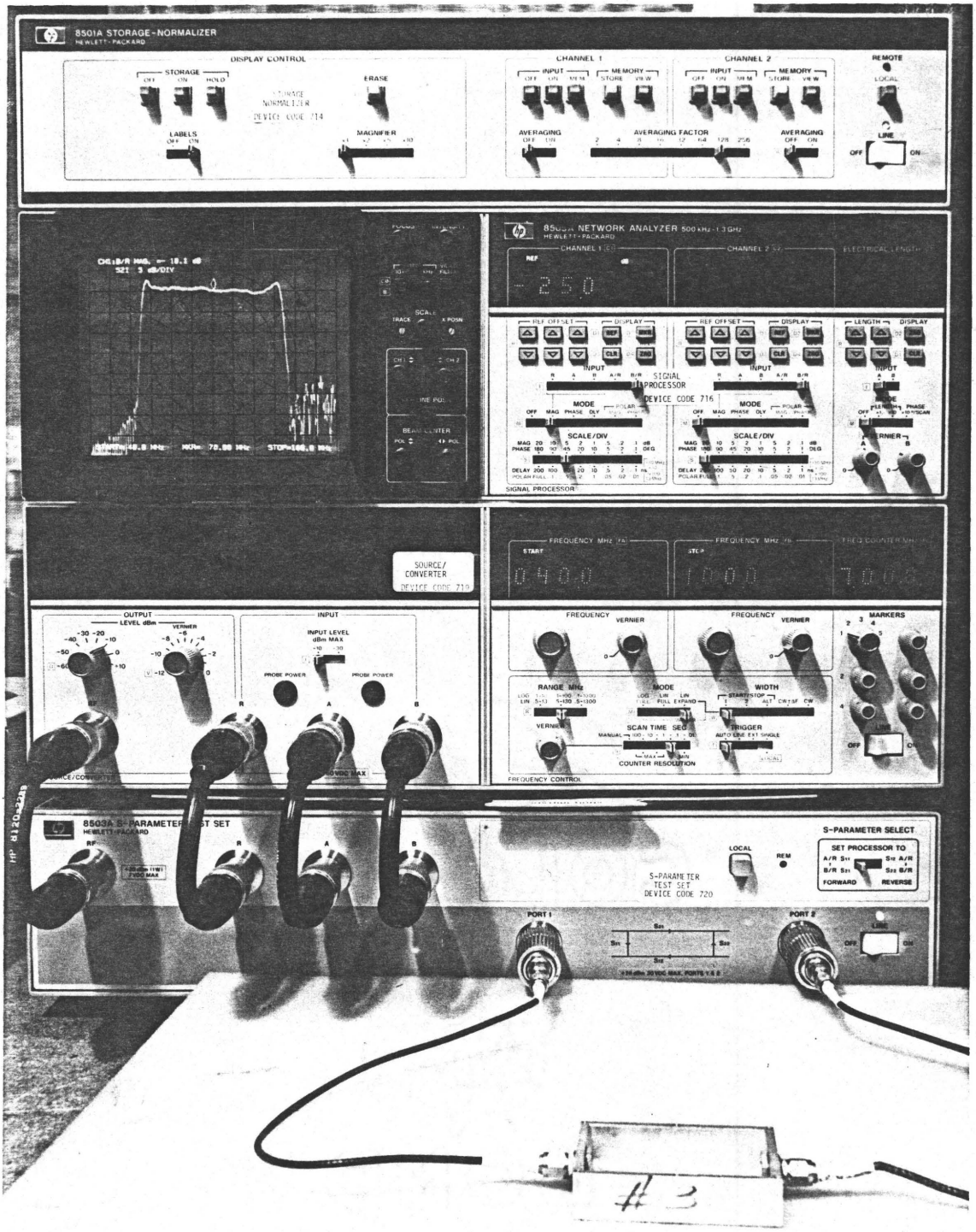

Figure 5.1 Photograph of Test Equipment

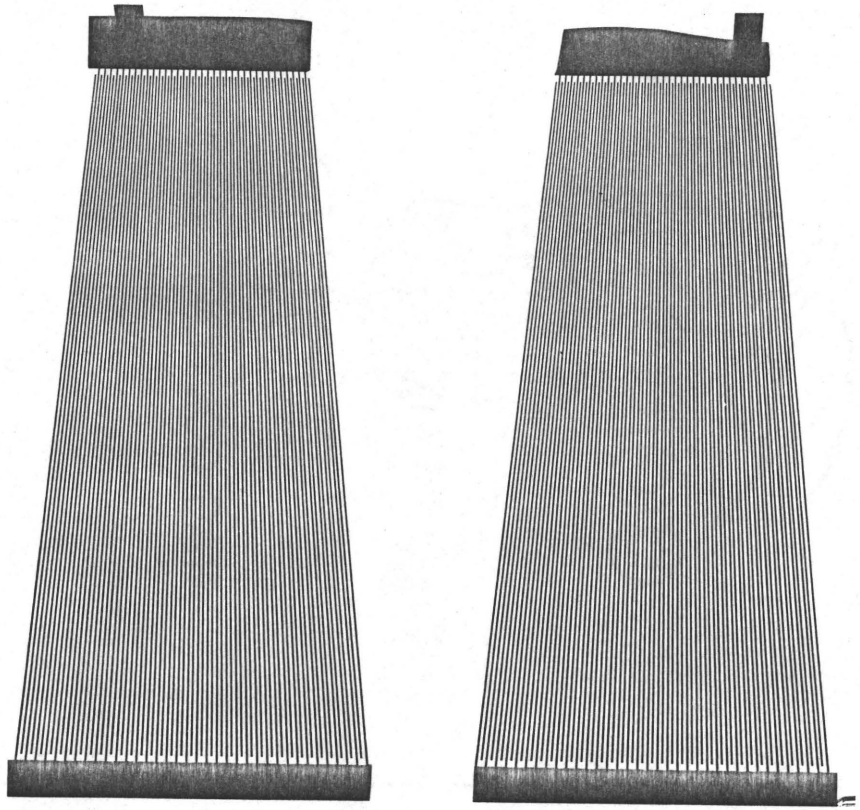

Figure 5.2 Slanted Finger Transducer Mask Pattern (20X)

Figure 5.3 Photograph of Slanted Finger Transducer SAW Filter (2.58X)

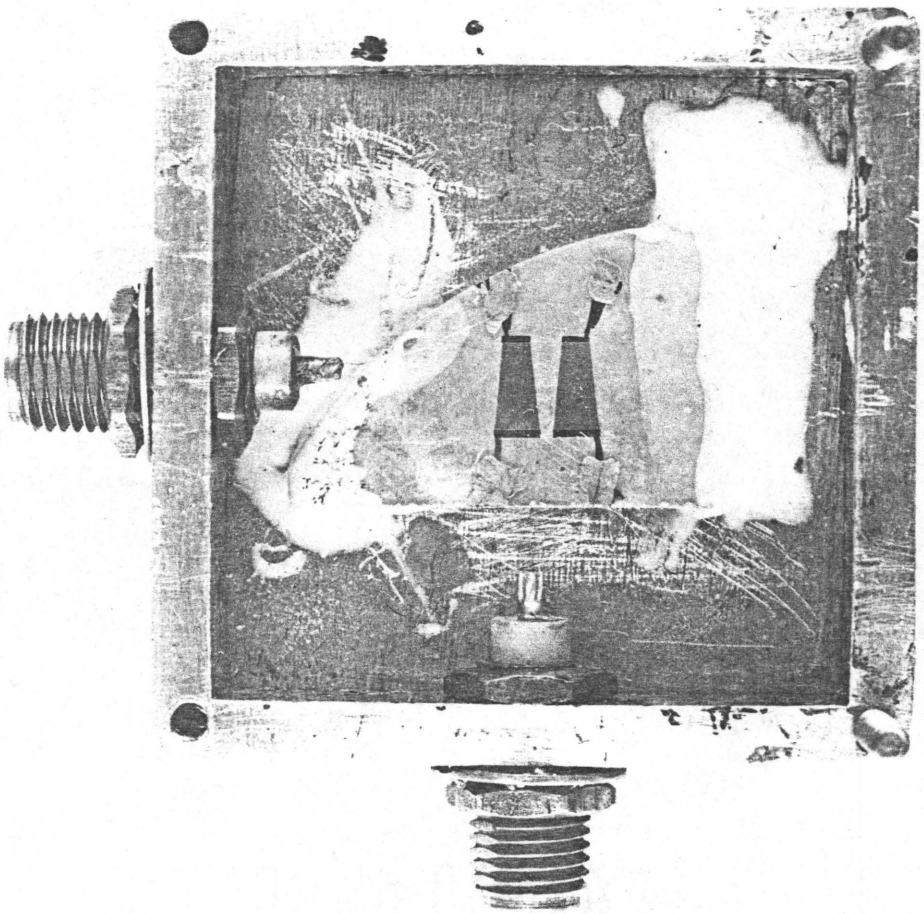

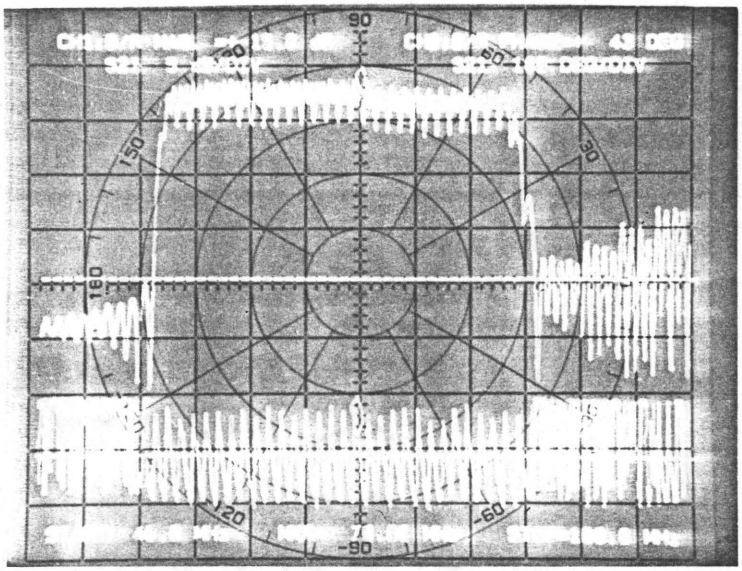

a)Ref = -52dB/120deg.

Figure 5.4 Slanted Finger Transducer SAW Filter Response

b)Ref = -36dB/120deg.

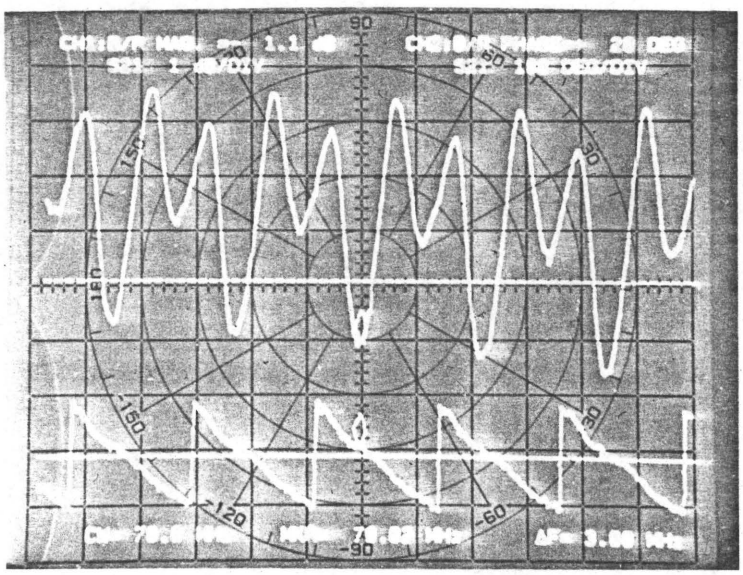

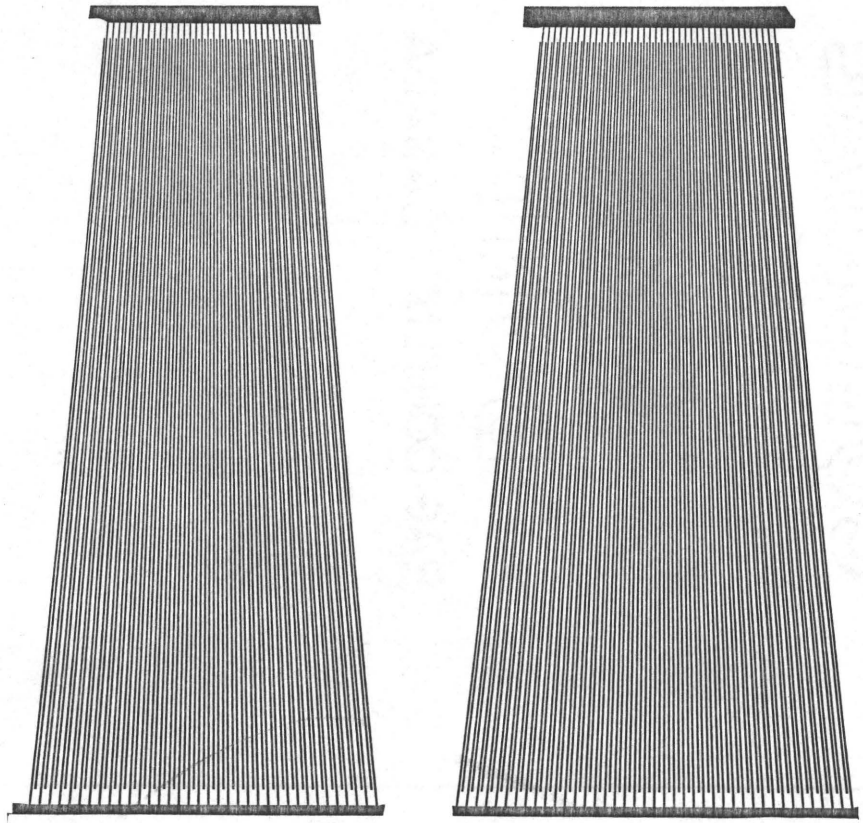

Figure 5.5 Curved Finger Transducer Mask Pattern (20X)

(p=-1/2)

Figure 5.6 Photograph of Curved Finger Transducer SAW Filter (2.6X)

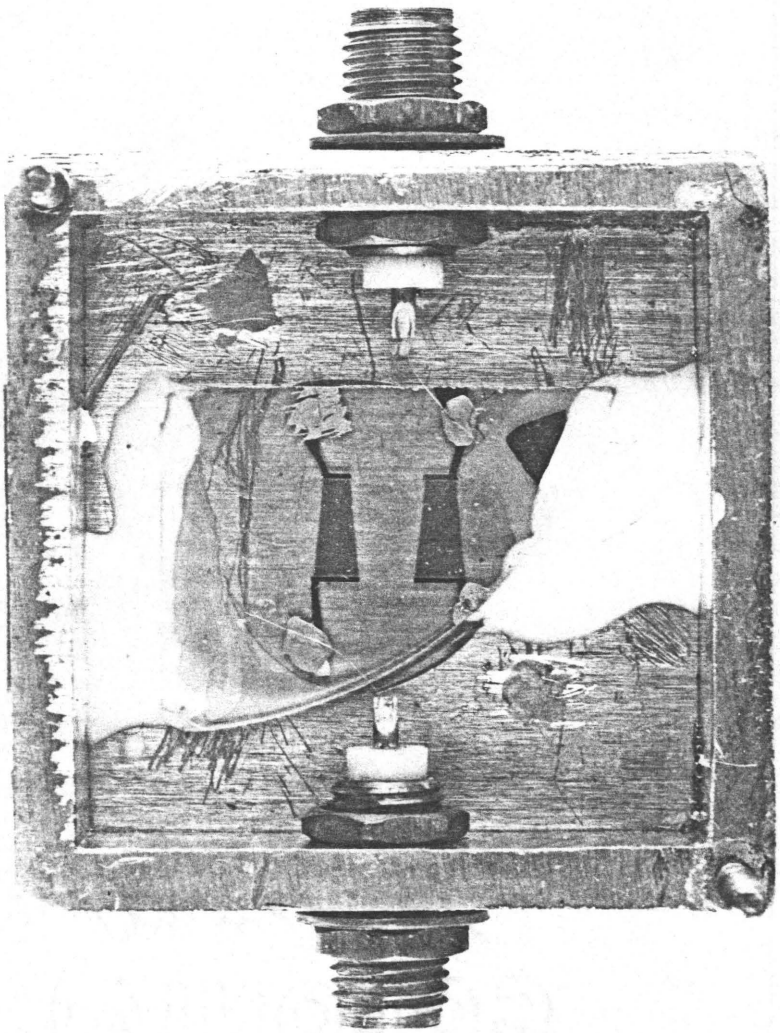

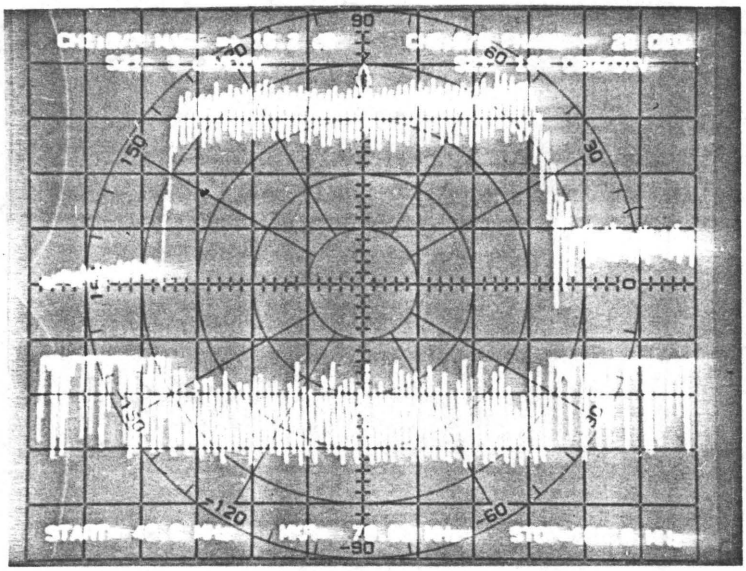

a) Ref = -60dB/120deg.

Figure 5.7 Curved Finger Transducer Filter Response

b) Ref = -45dB/120deg.

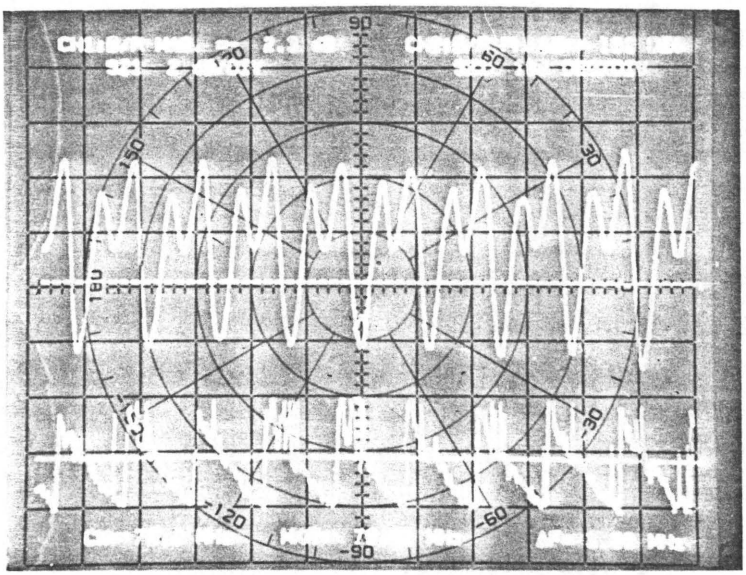

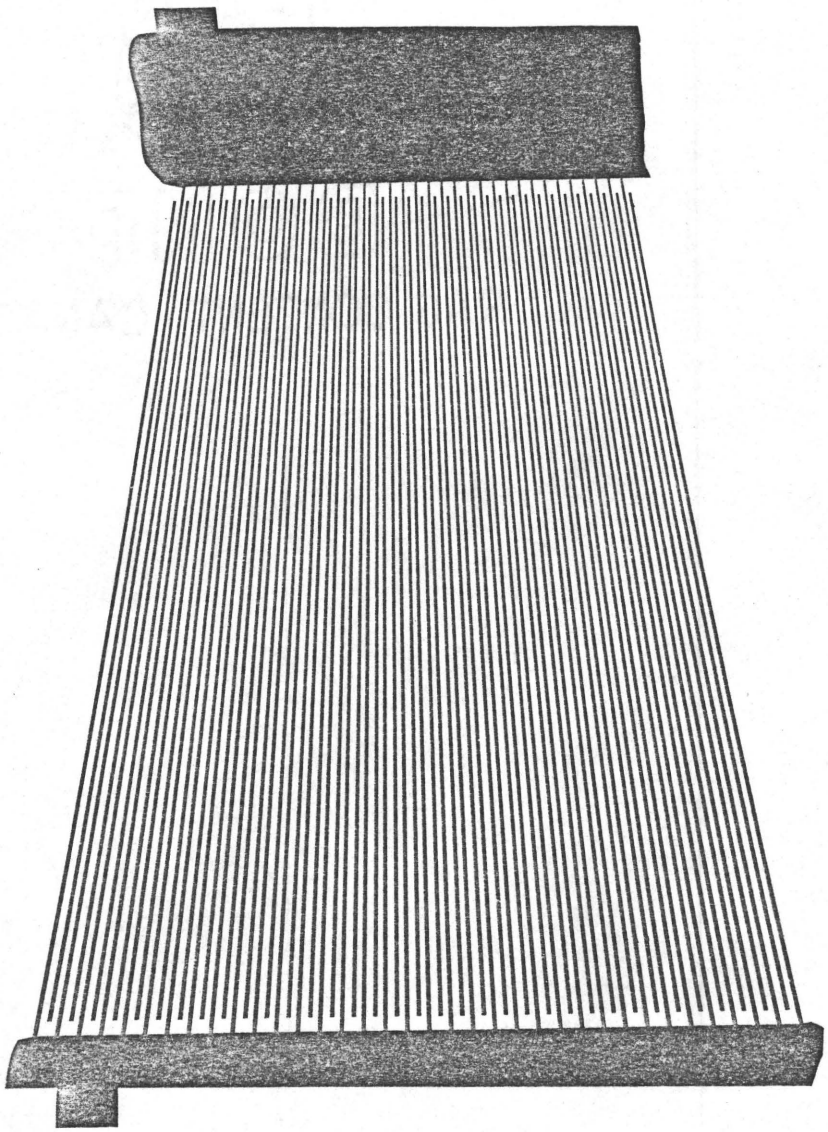

Figure 5.8 Curved Finger Transducer Mask Pattern (40.6X)

(p=-1/2)

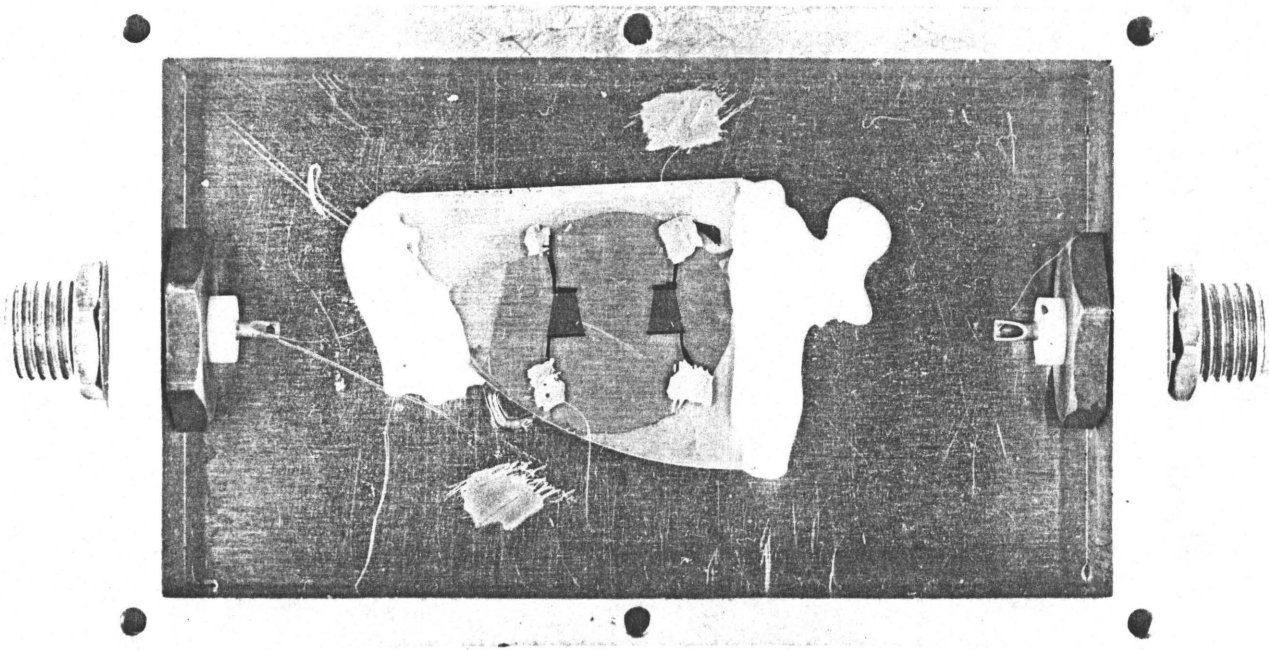

Figure 5.9 Photograph of Curved Finger Transducer SAW Filter (2X)

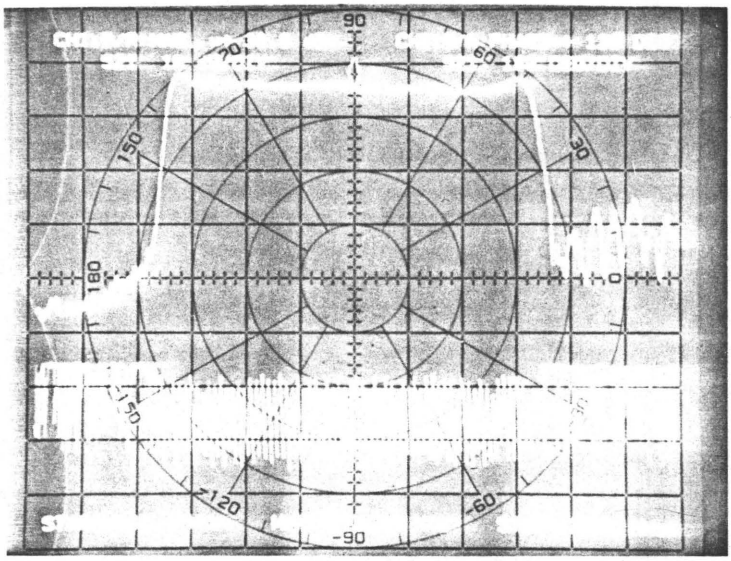

a) Ref = -07dB/120deg.

Figure 5.10 Curved Finger Transducer SAW Filter Response

b) Ref = -30.5dB/120deg.

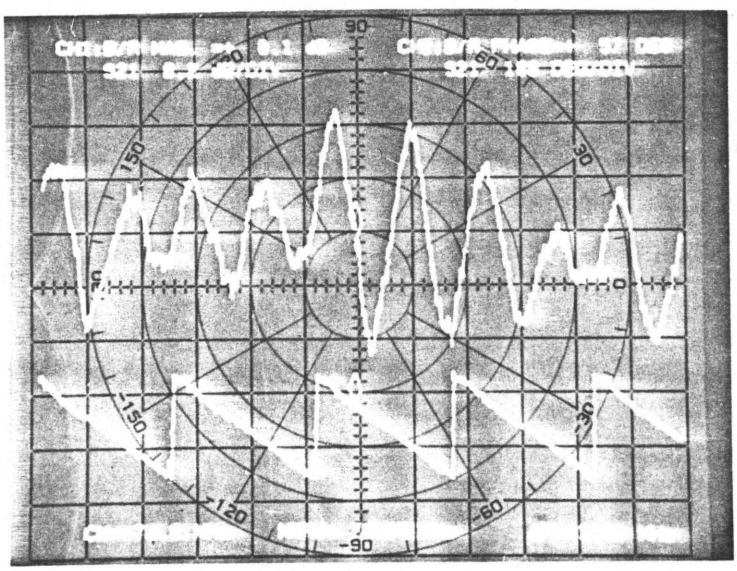

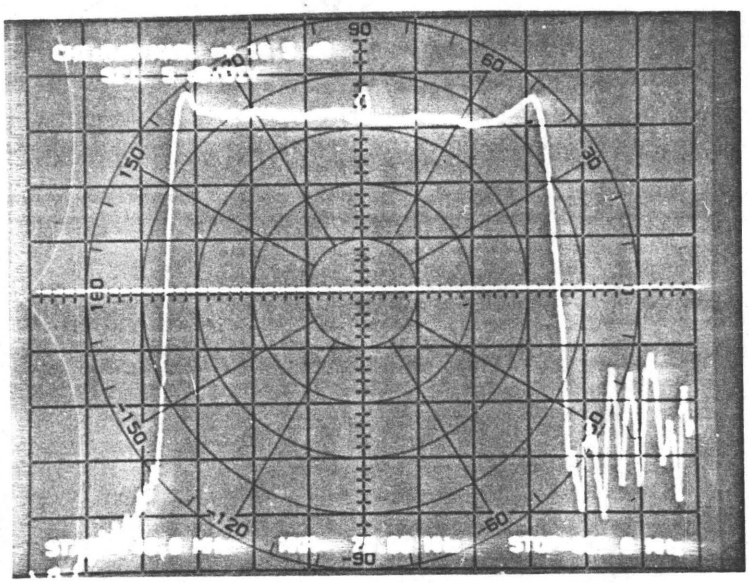

a) Ref = -67dB/120deg.

Figure 5.11 Half-sized Curved Finger SAW Filter Response

b) Ref = -30.5dB/120deg.

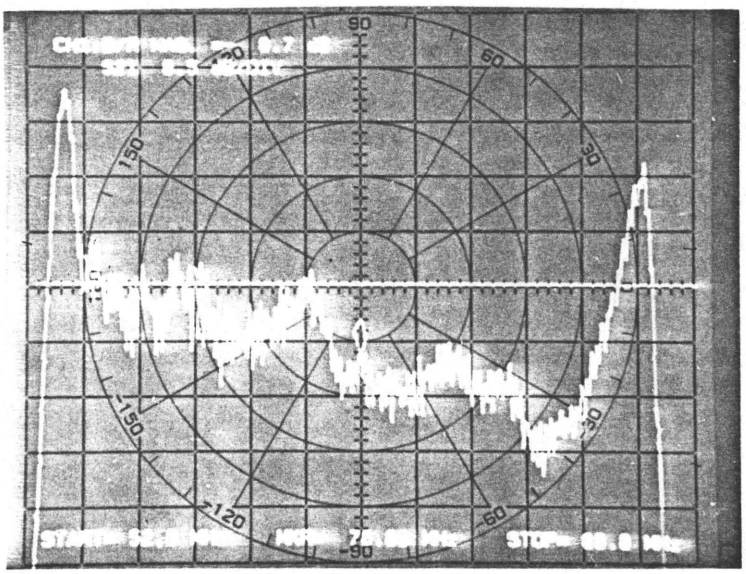

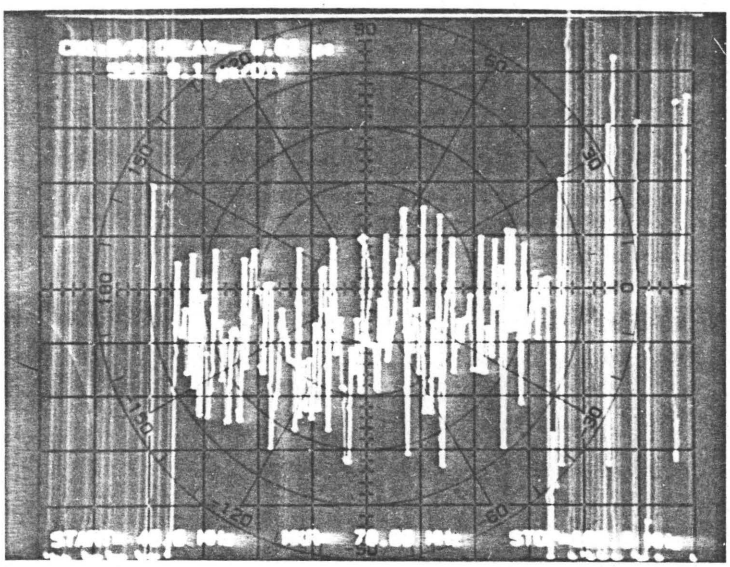

a) Group Delay Ref = +2.5us

Figure 5.12 Half-sized Curved Finger SAW Filter Response

b) SMITH CHART

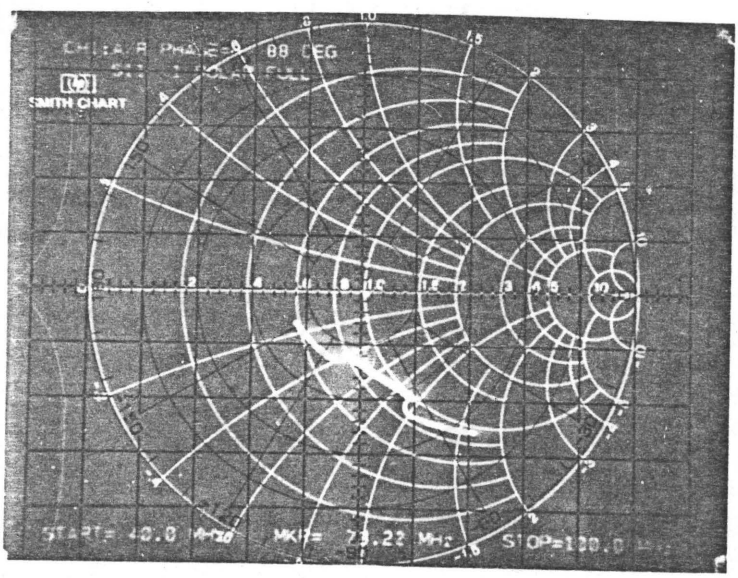

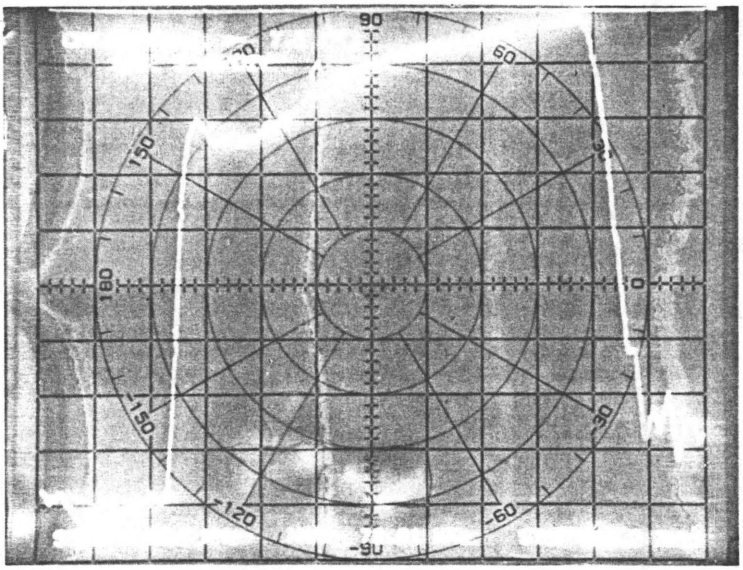

a) Ref = -25dB (p=1)

Figure 5.13 Illustrating Variation in Slope Attainable using Different Finger Curves

b) Ref = -20 dB (p=-1/2)

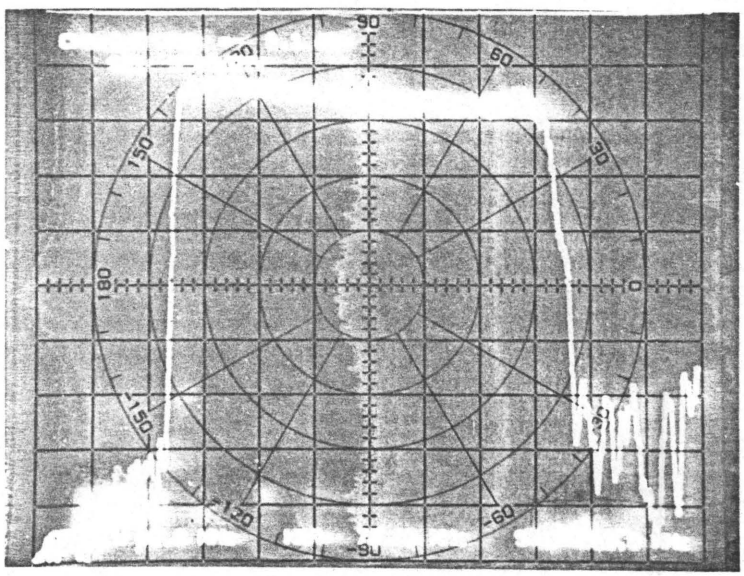

APPENDIX

The FORTRAN programs referred to in Section 4.2. are listed here. The first program, XMIT, is the routine used to convert a datafile representing a cutting sequence into a form which the SDK-8085 microprocessor can interpret. The convention for input consists of an ordered triplet (X,Y,P) where X and Y are the coordinates of a point on the cutting table surface in the range (0", 48"). P determines the status of the cutting knife, either up (P=0), or down and cutting (P=1). P also has the function of designating the end of data (EOD) mark (P=-1). The output convention is covered in Zeuner[23]; briefly, each relative move of the cutting knife is converted into a slope, the total number of motor steps, and a control word which indicates the direction of motion and the knife status.

The second program, MASK5, is representative of the routines used to create the datafiles for program XMIT. This particular program exhibits the versatility common to all such programs written in terms of ability to vary reduction ratio, number of finger pairs, acoustic aperture, percentage bandwidth, centre frequency, acoustic velocity and transducer separation. Also, the choice of single or double transducer digitisation with a change in parameters is available, if dissimilar transducers are to be cut.

The transducer cut is a curved finger variety with the curve specified by function statement, F(x). The basic form of the function

is

$$y = (N - SIGN/4.0)* v_a/[2 f_o(x)]$$

where v_a is the acoustic velocity and f_o the synchronous frequency. N determines the finger number in the range (-N0, N0) where N0 is the number of finger pairs, and SIGN determines the side of the finger being cut. The function statement in the program accounts for a change in origin by introducing offset parameters such that the initial actual starting position of the cutting knife is arbitrarily defined as the origin (0,0).

```
      PROGRAM XMIT(INPUT,OUTPUT,DATAF,TAPE1=DATAF,TAPE5=INPUT              &
     +,TAPE6=OUTPUT)
THIS PROGRAM READS IN UP TO 4000 DATA POINTS,PROCESSES
AND TRANSMITS THEM TO THE SDK-85 CUTTING TABLE CONTROL
SYSTEM FOR STORAGE ON CASSETTE TAPE.
      REAL MOVE(4000,3)
      INTEGER BUFSIZE,DIGITS(9),HEX(16),ECL,ECB
      DATA HEX/1H0,1H1,1H2,1H3,1H4,1H5,1H6,1H7,1H8,1H9                     &
     +,1HJ,1HK,1HL,1HM,1HN,1HC/
      DATA EOL,ECB/1HP,1H>/
      REWIND 1
    5 WRITE(6,10)
   10 FORMAT(10X," ENTER POINTS FROM DATA FILE(1) OR TERMINAL(5)?")
      READ(5,*)INPDEV
      IF(INPDEV.NE.1.AND.INPDEV.NE.5)GO TO 5
XOFSET,YOFSET,XSCALE,YSCALE PROVIDE FOR TRANSLATION
OF USER DATA UNITS TO CUTTING TABLE UNITS
      XOFSET=0.0
      YOFSET=0.0
      XSCALE=2000.0
      YSCALE=2000.0
      WRITE(6,20)
   20 FORMAT(10X," ENTER DATA IN FORM (X,Y,P),WITH X,Y IN INCHES",/,      &
     +10X," P=0  (MOVE)  ,P=1  (DRAW)  ,P=-1  (END OF DATA)",/,           &
     +10X," X,Y DATA MUST BE IN RANGE 0-48 INCHES")
*N* KEEPS TRACK OF THE NUMBER OF ENTERED POINTS
      N=0
   30 N=N+1
      READ(INPDEV,*)X,Y,P
      IF(X.LT.0.0.OR.X.GT.48.0.OR.Y.LT.0.0.OR.Y.GT.48.0)GO TO 40
      IF(P.NE.-1.0.AND.P.NE.0.0.AND.P.NE.1.0)GO TO 40
      MOVE(N,1)=X
      MOVE(N,2)=Y
      MOVE(N,3)=P
      IF(P.EQ.-1.0)GO TO 60
      GO TO 30
   40 WRITE(6,50)N
   50 FORMAT(10X," ERROR IN INPUT DATA,RE-ENTER POINT ",I6)
      N=N-1
      IF(INPDEV.EQ.1)STOP
      GO TO 30
*N* NOW REPRESENTS THE TOTAL NUMBER OF ENTERED POINTS
   60 WRITE(6,70)N
   70 FORMAT(10X,I6," POINTS ENTERED")

PRESCALE INPUT DATA TO CUTTING TABLE UNITS
      DO 90 I=1,N
      MOVE(I,1)=(MOVE(I,1)-XOFSET)*XSCALE
      MOVE(I,2)=(MOVE(I,2)-YOFSET)*YSCALE
   90 CONTINUE
CONVERT DATA TO A SERIES OF MOVES AND DRAWS,SUCH THAT
MOVE(I,1)  : THE MAGNITUDE OF THE CHANGE
             IN THE X COORDINATE
MOVE(I,2)  : THE MAGNITUDE OF THE CHANGE
             IN THE Y COORDINATE
MOVE(I,3)  : CONTAINS INFORMATION CONCERNING
             WHETHER THE X OR Y INCREMENT IS LARGER
             IN MAGNITUDE,WHETHER TO MOVE OR DRAW,
             AND THE DIRECTION OF THE NEW MOTION.
      NM1=N-1
      DO 100 I=1,NM1
      J=I+1
      DELTX=MOVE(J,1)-MOVE(I,1)
      DELTY=MOVE(J,2)-MOVE(I,2)
```

```
      P=MOVE(J,3)
SET UP CONTROL(CNTL)BYTE :
           B0= DRAW ,B1= X POSITIVE ,B2= Y POSITIVE ,B3= Y > X
      MOVE(I,3)=0.0
      IF(ABS(DELTX).LT.ABS(DELTY))MOVE(I,3)=MOVE(I,3)+8.0
      IF(DELTY.GE.0.0)MOVE(I,3)=MOVE(I,3)+4.0
      IF(DELTX.GE.0.0)MOVE(I,3)=MOVE(I,3)+2.0
      IF(P.EQ.1.0)MOVE(I,3)=MOVE(I,3)+1.0
      MOVE(I,1)=ABS(DELTX)
      MOVE(I,2)=ABS(DELTY)
100   CONTINUE
MICROCOMPUTER BUFFER CAN HOLD BLKSIZE/5 MOVES AT A TIME
WHERE BLKSIZE=(HIGHEST - LOWEST BUFFER LOCATION)
CONVENTION FOR OUTPUT TO SDK-85 MICROCOMPUTER
IS AS FOLLOWS :
     DIGITS(5-8) :HEXIDECIMAL DIGITS FOR MAXIMUM NUMBER
                  OF 1/2000TH INCH STEPS
     DIGITS(1-4) :HEXIDECIMAL DIGITS FOR FRACTIONAL
                  EQUIVALENT OF MINIMUM NUMBER OF
                  1/2000TH INCH STEPS
     DIGITS(9)   :HEXIDECIMAL CNTL BYTE
      BUFSIZE=200
      K=0
      DO 130 I=1,NM1
K POINTS TO DATA LOCATION MODULO BUFSIZE
      IF(K.EQ.BUFSIZE)K=0
      J=1
      SLOPE=0.0
      IF(MOVE(I,1).EQ.0.0.OR.MOVE(I,2).EQ.0.0)GO TO 13
      SLOPE=MOVE(I,1)/MOVE(I,2)
      IF(SLOPE.EQ.1.0)SLOPE=.999999999
      IF(SLOPE.GT.1.0)SLOPE=1.0/SLOPE
 13   IF(MOVE(I,1).LT.MOVE(I,2))J=2
      ZSCALE=XSCALE
      IF(J.EQ.2)ZSCALE=YSCALE
      ZOFSET=XOFSET
      IF(J.EQ.2)ZOFSET=YOFSET
      LOOK1=1
      IF(MOVE(I,J).GT.(32.0-ZOFSET)*ZSCALE)LOOK1=2
      IF(MOVE(I,J).GT.(32.0-ZOFSET)*ZSCALE)MOVE(I,J)=MOVE(I,J)/2.0
CONVERT MOVES TO HEXADECIMAL
      DIGITS(5)=INT(MOVE(I,J)/4096.)
      DIGITS(6)=INT(MOVE(I,J)/256.)-DIGITS(5)*16
      DIGITS(7)=INT(MOVE(I,J)/16.)-DIGITS(6)*16-DIGITS(5)*256
      DIGITS(8)=INT(MOVE(I,J))-DIGITS(7)*16-DIGITS(6)*256
     +-DIGITS(5)*4096
      DIGITS(1)=INT(SLOPE*16.)
      DIGITS(2)=INT(SLOPE*256.0)-DIGITS(1)*16
      DIGITS(3)=INT(SLOPE*4096.0)-DIGITS(2)*16-DIGITS(1)*256
      DIGITS(4)=INT(SLOPE*65536.0)-DIGITS(3)*16-DIGITS(2)*256
     +-DIGITS(1)*4096
      DIGITS(9)=MOVE(I,3)
CONVERT TO "HEXIDECIMAL" FOR OUTPUT
      DO 110 L=1,9
      DIGITS(L)=HEX(DIGITS(L)+1)
110   CONTINUE
WAIT FOR MICROCOMPUTER,IF AT BEGINNING OF NEW BUFFER
      IF(K.NE.0)GO TO 115
125   WRITE(6,127)
      READ(5,126)SIGNL
      IF(SIGNL.NE."GO")GO TO 125
126   FORMAT(A2)
127   FORMAT(" WAITING FOR "GO" SIGNAL FROM MICROCOMPUTER")
115   DO 116 LOOK2=1,LOOK1
      K=K+1



      IF(I.NE.NM1.AND.K.LT.BUFSIZE)WRITE(6,120)DIGITS,ECL
116   IF(I.EQ.NM1.OR.K.GE.BUFSIZE)WRITE(6,120)DIGITS,EOB
120   FORMAT(1X,10A1)
IF END OF BUFFER BUT NOT END OF DATA
SEND END OF BUFFER SIGNAL,"E"
      IF(K.GE.BUFSIZE.AND.I.NE.NM1)WRITE(6,122)
IF END OF DATA SEND END OF DATA SIGNAL,"T"
      IF(I.EQ.NM1)WRITE(6,121)
121   FORMAT(" T")
122   FORMAT(" E")
130   CONTINUE
      END
```

```
      PROGRAM MASK5(INPUT,OUTPUT,DATA4,                                 5
     +TAPE1=DATA4,TAPE5=INPUT,TAPE6=OUTPUT)
C THIS PROGRAM CALCULATES THE COORDINATES FOR A CURVED
C FINGER SAW FILTER MASK AND OUTPUTS THEM TO TAPE1.
C FINGERS ARE SYMMETRIC ABOUT THE X-AXIS.
C DIGITISATION FOLLOWS CUTTING PROCEDURE:
C    1. STARTING POINT OF INPUT TRANSDUCER IS OUTPUT
C    2. LOWER SIDE OF LH ELEMENT OF FINGER PAIR IS OUTPUT,
C       USING SAW. CURVE.
C    3. RH EDGE OF FINGER IS OUTPUT.
C    4. UPPER SIDE OF LH ELEMENT IS OUTPUT.
C    5. STARTING POINT FOR NEXT FINGER PAIR IS OUTPUT.
C    6. PROCEDURE REPEATS FOR ALL LH ELEMENTS.
C    7. PROCEDURE IS EXECUTED IN REVERSE FOR RH ELEMENTS.
C    8. PROCEDURE REPEATS FOR OUTPUT TRANSDUCER
C    9. ORIGINAL START POSITION IS OUTPUT,ALONG WITH
C       END OF DATA ( EOI ) MARK.
C
C         (ALL DIMENSIONS IN INCHES)
      F(X)=C1+(FLOAT(N)-SIGN/4.0)*C2*(X+C3)*(X+C3)
C INITIALISATION OF PLOTTING
      REWIND 1
      X=0.0
      Y=0.0
      PU=0.0
      PD=1.0
      EOI=-1.0
      WRITE(1,1)X,Y,PU
    1 FORMAT(3(3X,F8.5))
C INITIALISATION OF CONTROLLING PARAMETERS
      SCALE=7.5*70./3.488/3.937/2.
      SCALE=5.0
      NSTRP=10
      GAP=SCALE*0.03
      ETA=0.5
      N0=40
      W=SCALE*2.0
      BW=0.5
      FC=70.0E+06
      V=SCALE*3488.0*39.37*20.0
      XOFSET=SCALE*0.2
      YOFSET=SCALE*0.2
      SEP=SCALE*0.4
C SINGLE TRANSDUCER J = 1 : DOUBLE TRANSDUCER J = 0
      J=1
      X=XOFSET
      Y=YOFSET
C CALCULATION OF INTERMEDIATE PARAMETERS
    5 DELTF=BW*FC
      DELTX=W/FLOAT(NSTRP)
      FHI=FC+DELTF/2.0
      FLO=FC-DELTF/2.0
      C3=W/(SQRT(FLO/FHI)-1.0)
      C1=YOFSET+(FLOAT(N0)+.25)*V/2.0/FLO*(1.-GAP/C3)*(1.-GAP/C3)
      C2=V/(2.0*C3*C3*FLO)
      C3=C3-(XOFSET+GAP)
      WRITE(1,1)X,Y,PU
C DIGITISE LH ELEMENTS,STARTING AT BOTTOM.
      K=0
      N=-N0
      SIGN=-1.0
   10 CONTINUE
C LOWER SIDE OF FINGER.
      Y=F(X)
```

```
      WRITE(1,1)X,Y,PD
      X=X+SIGN*GAP
      Y=F(X)
      WRITE(1,1)X,Y,PD
      DO 20 I=1,NSTEP
      X=X+SIGN*DELTX
      Y=F(X)
      WRITE(1,1)X,Y,PD
   20 CONTINUE
      SIGN=-SIGN
      Y=F(X)
      WRITE(1,1)X,Y,PD
C UPPER SIDE OF FINGER.
      DO 30 I=1,NSTEP
      X=X+SIGN*DELTX
      Y=F(X)
      WRITE(1,1)X,Y,PD
   30 CONTINUE
      X=X+SIGN*GAP
      Y=F(X)
      WRITE(1,1)X,Y,PD
      ISIGN=INT(SIGN)
      N=N-2*ISIGN
      SIGN=-SIGN
      IF(IABS(N).LE.N0)GO TO 10
C FINISHED FINGERS ON THIS SIDE
      IF(K.NE.0)GO TO 40
C START RHS OF TRANSDUCER
      Y=X+GAP+W+GAP
      WRITE(1,1)X,Y,PU
      K=1
      N=N0-1
      SIGN=-1.0
      GO TO 10
   40 CONTINUE
      IF(J.NE.0)GO TO 50
      X=XOFSET
      Y=2.0*C1-YOFSET+SEP
      NC=35
      J=1
      YOFSET=Y
      GO TO 5
C FINISHED MASK
   50 X=0.0
      Y=0.0
      WRITE(1,1)X,Y,EOD
      END
```

BIBLIOGRAPHY

1. Arfken, G., Mathematical Methods for Physicists, 2nd Ed., Academic Press, New York, 1970, p. 414, 542.

2. Bell, D.T. and Claiborne, L.T., Phase Code Generators and Correlators, in MATTHEWS, p. 321.

3. Campbell, C.K. et al., "Wideband Linear Phase SAW Filter Design using Slanted Finger Transducers", to be published in IEEE Trans. Sonics Ultrasonics.

4. El-Diwany, M.H., "Surface Acoustic Wave Bandpass Filter Synthesis and Design", M.Eng. Thesis, McMaster University, May 1975.

5. Farnell, G.W., "Elastic Surface Waves", in Matthews, p. 1

6. Hartmann, C.S. et al., "Impulse Model Design of Acoustic Surface Wave Filters", IEEE Trans. MTT-21, 162 (1973).

7. Kraus, J.D. and Carver, K.R., "Electromagnetics", 2nd Ed., McGraw-Hill, New York, 1973, p. 85, 114, 162.

8. Maissel, L.I. and Glang, R., "Handbook of Thin Film Technology", McGraw-Hill, 1970, Chapter 7.

9. Mason, W.P., "Electromechanical Transducers and Wave Filters", 2nd ed., Van Nostrand, New York, 1948, p. 200, 399.

10. Matthews, H. (ed.), Surface Wave Filters, Wiley, New York, 1977.

11. Milsom, R.F., "Bulk Wave Generation by the IDT", Wave Electronics, 2, 64 (1976).

12. Milsom, R.F. et al., "The Interdigital Transducer", in Matthews, p. 55.

13. Naraine, P.M., "Design and Synthesis of Harmonic Surface Acoustic Wave Delay Lines", M.Eng. Thesis, McMaster University, Sept. 1980.

14. Omar, M.A., Elementary Solid State Physics, Addison Wesley, Phillipines, 1975, p. 406.

15. Ruoff, A.L., Introduction to Materials Sciences, Prentice-Hall, New Jersey, 1972, p. 119, 263.

16. Seiler, D.G., "Design and Synthesis of a VHF Surface Acoustic Wave Oscillator", M.Eng. Thesis, McMaster University, Dec. 1975.

17. Smith, H.I., "Surface Wave Device Fabrication", in Matthews, p. 165.

18. Smith, W.R. et al., "Analysis of Interdigital Surface Wave Transducers by use of an Equivalent Circuit Model", IEEE Trans. MTT-17, 856 (1969).

19. Smith, W.R., "Basics of the SAW Interdigital Transducer", Wave Electronics, 2, 25 (1976).

20. Snow, P.G., "Matching Networks and Packaging Structures", in Matthews, p. 219.

21. Tancrell, R.H., "Principles of Surface Wave Filter Design", in Matthews, p. 109.

22. Williamson, R.C., "Reflection Grating Filters", in Matthews , p. 386.

23. Zeuner, A.N., "A Microprocessor-Controlled Cutting Table", M.Eng. Project Report, to be published.